Dynamics of Exchange at Gas–Zeolite Interfaces I: Pure Component n-Butane and Isobutane

M. Chandross[1], E.B. Webb III[1], G.S. Grest[1],
M.G. Martin[2], A.P. Thompson[2], and M.W. Roth[3]

[1]*Mail Stop 1411, Sandia National Laboratories, Albuquerque, NM 87185*

[2]*Mail Stop 1111 Sandia National Laboratories, Albuquerque, NM 87185*

[3]*Texas A&M University, Department of Physical and Life Sciences, Corpus Christi, TX 78412*

(June 30, 2000)

Abstract

We present the results of molecular dynamics simulations of n-butane and isobutane in silicalite. We begin with a comparison of the bulk adsorption and diffusion properties for two different parameterizations of the interaction potential between the hydrocarbon species, both of which have been shown to reproduce experimental gas-liquid coexistence curves. We examine diffusion as a function of the loading of the zeolite, as well as the temperature dependence of the diffusion constant at loading and for infinite dilution. We continue with simulations in which interfaces are formed between single component gases and the zeolite. After reaching equilibrium, we examine the dynamics of exchange between the bulk gas and the zeolite. Finally, we calculate the permeability of the zeolite for n-butane and isobutane as a function of pressure. Our simulations are performed for a number of different gas temperatures and pressures, covering a wide range of state points.

I. INTRODUCTION

Zeolites are microporous materials that are ideally suited to a number of different industrial applications such as catalytic cracking or hydroisomerization of hydrocarbon molecules as well as ion exchange in dessicant or purification applications. Zeolites with medium pore sizes, such as silicalite (structure type MFI) [1], are additionally useful for separations processes, as their openings are approximately the same size as the kinetic diameter of many small molecules. As such, the utility of any given zeolite in a separations application is strongly dependent on the preferential adsorption, as well as the relative diffusivities of the sorbed species.

There exists a large body of theoretical [2–6] and experimental [7–14] work that investigates the diffusion properties of small alkanes in zeolites. Simulations are generally performed with either Molecular Dynamics (MD) or Monte Carlo (MC) methods [15], both of which give calculated diffusivities that agree well with each other, although the MC methods, not having a true time dependence, rely on transition state theory for rate constants. The experimental situation is much less clear. Experimental diffusion constants can be measured through both microscopic and macroscopic methods, with the calculated diffusivities differing by an order of magnitude or more between the two methods. While macroscopic studies measure the diffusion of the molecules indirectly, as in supported membrane studies where the diffusion is calculated from the permeation flux, the microscopic measurements directly follow the mean-squared displacement of individual molecules. This is the same method that is used in simulations, and it is for this reason that simulations tend to agree more with microscopic diffusion studies rather than macroscopic. It has been suggested that the difference between the macroscopic and microscopic measurements lies in the improper assumption of Fickian diffusion in the former [16] or the difference between the diffusion of gas-phase and adsorbed components [17], but this discussion lies outside the scope of this paper. With the above in mind, when both macroscopic and microscopic measurements are available for comparison with our simulations, we only use the microscopic measurements.

DISCLAIMER

DISCLAIMER

Portions of this document may be illegible in electronic image products. Images are produced from the best available original document.

Simulations of molecular adsorption on zeolites have traditionally been MC studies of adsorption isotherms [18–22]. While Monte Carlo methods are much more efficient for computing equilibrium properties of the gas/zeolite system than MD, MC is not well suited for calculating time dependent properties. We are primarily interested in the dynamics of exchange between the gas and adsorbed phases through direct analysis of molecular trajectories which are not available from MC interface simulations. In fact, while our MC studies include a gas phase in the simulation, most do not, instead relying on parameterized equations of state that equate a calculated chemical potential with a gas pressure [22]. It is for these reasons that we have focused our studies on MD simulations. We have verified that MD simulations equilibrate to the state points as given by the adsorption isotherms from MC (see below). With the demonstrated success of MD simulations in both the gas and the zeolite, as well as at the interface (i.e. adsorption isotherms), we feel that the specifics of molecular exchange between the gas and the zeolite are equally well represented, and elucidate the dynamics of a process that can not presently be investigated experimentally.

For this work, we restrict ourselves to n-butane (hereafter butane) and isobutane. The use of these small molecules avoids the computational burden associated with longer molecules, while still allowing us to compare fast and slow diffusing species.

The remainder of the paper is arranged as follows: In section II we present the details of our simulation methodology, including descriptions of the parameter sets used. We continue in section III with the results of our simulations of bulk zeolite crystals. These include adsorption isotherms and diffusion studies. Our interface simulations are presented in IV, where we examine the exchange dynamics for systems in equilibrium. We present non-equilibrium permeation studies, in which a concentration gradient appears on either side of the zeolite membrane in section V. We conclude and discuss our future work in section VI.

II. SIMULATION DETAILS

We perform MD simulations of butane and isobutane using an united atom (UA) representation for the CH_n groups, in which each group is treated as a single pseudo-atom. We used two different simulation codes, one of which constrained all C-C bond lengths to 1.54 Å using the RATTLE algorithm [15], while the other used a harmonic potential between UAs with a spring constant of 452,900 K/Å^2 [23]. The simulations with the constrained bonds used a 5 fs timestep and a Langevin thermostat. Those with the harmonic potential used a multiple time step rRESPA algorithm [24] with a 1.25 fs timestep for the bonds, a 2.5 fs timestep for the angles, and a 5 fs timestep for the interaction between non-bonded CH_n UAs with temperature control via a Nosé-Hoover thermostat. The former simulations were run with the same code as in our previous work [3,25,26], while the latter were run with the large-scale parallel MD code LAMMPS [27]. We have verified that these two different approaches equilibrate to the same points on the isotherms. We have found slight differences in the exchange dynamics between the two codes when run as described above. These differences, however, disappeared when both codes were implemented with a Langevin thermostat demonstrating that covalent bond representation was not the cause. For technical reasons the multi-time step rRESPA algorithm is not presently implemented with Langevin dynamics. Hence, to compare differences between exchange dynamics from Nosé-Hoover and Langevin thermostats, simulations were run with both codes using a single time step of 1.25 fs. A Nosé-Hoover thermostat is essentially a velocity rescaling scheme, which adds no randomness to the system – velocities of all particles are scaled so as to make the kinetic temperature match the prescribed temperature. This type of thermostat is most applicable in dense systems, such as liquids, where frequent molecular collisions serve to randomize velocities. The Langevin thermostat, on the other hand, couples the particles to a heat bath via a random force and viscous damping, which are coupled through the fluctuation-dissipation theorem. The Langevin thermostat is most appropriate for our interface simulations, as it simulates both collisions with a carrier gas as well as the effect

of a vibrating crystal lattice for molecules sorbed inside the zeolite. It is for these reasons that most of our simulations are performed with a Langevin thermostat, especially where dynamical information is desired.

Both codes include three body bending and four body torsion terms [15] of the forms below.

$$V_b(\theta) = \frac{k_b}{2}(\theta - \theta_b)^2 \tag{1}$$

$$V_t(\phi) = \sum_i a_i \cos^i(\phi) \tag{2}$$

where k_b is the angular spring constant, θ (θ_b) is the (equilibrium) angle between three neighboring atoms, and ϕ is the torsional angle as described in Ref. [15]. All non-bonded interactions are governed by a 12-6 cut and shifted Lennard-Jones (LJ) interaction

$$V_{LJ}(r) = 4\epsilon[(\frac{\sigma}{r})^{12} - (\frac{\sigma}{r})^6] \tag{3}$$

Unless otherwise indicated, we use a cutoff of $r_c = 10$ Å. For the adsorption isotherms in section III A we also present results for larger values of the cutoff, $r_c = 14$ Å and 18 Å. We use two different parameterizations for the LJ interactions, both developed by Siepmann and coworkers to accurately predict vapor-liquid coexistence curves for linear and branched alkanes of various lengths [28–33] (see Tables I and II). We refer to these parameterizations as mSKS (modified Siepmann, Karaborni, Smit) [28–31] and TraPPE (Transferable Potentials for Phase Equilibria) [32,33], respectively. In both force fields, methyl, methylene, and methine groups are described by a single set of parameters regardless of their neighbors. Note that while this is the prescription for the TraPPE force field, the original SKS force field had a methyl group whose parameters depended upon its neighbors. To reduce confusion we refer to our SKS force field (i.e. with constant methyl group parameters) as mSKS.

The reason for using two different potential sets is two-fold. First, while the TraPPE force field reproduces the experimental vapor-liquid coexistence curves better than SKS, it is unknown how the two sets compare for dynamical measurements, such as diffusion

	TraPPE & mSKS	Units
bond length	1.54	$\AA$
k_b (bending)	124.18	kcal/(mol rad^2)
θ_b	114.0^o	
a_0 (torsion)	2.007	kcal/mol
a_1	4.012	
a_2	0.271	
a_3	-6.290	

TABLE I. Lennard-Jones potential parameters.

Model	Group	σ ($\AA$)	ϵ (kcal/mol)
TraPPE	CH_3	3.750	0.195
	CH_2	3.950	0.0914
	CH	4.680	0.0199
mSKS	CH_3	3.930	0.227
	CH_2	3.930	0.093
	CH	3.850	0.064

constants. Second, our previous work on the diffusion of long linear and branched alkanes used the mSKS potential set [3,25,26], and this study can help to understand how the results from that work relate to the new potential set.

The zeolite structure in our simulation is taken from the database contained in the Insight II software from Molecular Simulations, Inc. [34], and is assumed to be rigid. The LJ interaction between the atoms of the zeolite and the UAs of the alkanes is taken from the work of June et al. [35], with a slight modification. In the original work, all UAs (i.e. CH_3 and CH_2) were treated as identical units. For this work we have normalized this interaction to decane in order to arrive at separate parameters for the different UAs, as described previously [3,26]. These parameters are not optimized for diffusion or adsorption and thus perform adequately at best, particularly for isobutane, but this is not of concern as our primary purpose is to compare the dynamics within the given alkane models, using the same alkane/zeolite interaction.

Isotherms were computed using a combination [36,37] of coupled-decoupled [33] configurational-bias MC simulations [38–41] and the isobaric-isothermal version of the Gibbs ensemble [42–44]. One simulation box contained 12 unit cells of silicalite and was kept at a constant volume, while the other simulation box exchanged volume with an external pressure bath. The system contained 400 solute molecules which were allowed to exchange between the two simulation boxes. Simulations were run for 10,000 cycles, where each cycle consisted of 400 MC moves. Moves were chosen at random with a fixed probability of performing a volume move (0.01), molecule exchange (0.19), molecule regrowth (0.2), translation of the center of mass (0.3), and rotation about the center of mass (0.3). The maximum volume, translational, and rotational displacements were automatically adjusted to achieve an acceptance rate of 50%.

For our diffusion studies, our zeolite crystal contained 96 unit cells, four each in the (100) and (001) directions, and six in the (010) direction. Periodic boundary conditions were applied in all directions. For all diffusion studies guest molecules were inserted along the straight channels of the zeolite, and allowed to diffuse at high temperature (e.g. $T = 900K$).

The temperature was gradually reduced to the desired temperature for a given run, and the system was then allowed to equilibrate before data were taken. In the dilute limit (i.e. non-interacting sorbate molecules) we simulated 96 molecules, while for finite density the number of molecules ranged from 96 to 768. Our interface runs used the same zeolite crystal as the diffusion studies with the addition of a large ($\sim$ 100 Å) gas region alongside the (010) crystal face. Our interface simulations were performed in three stages. The first stage was a gas equilibration run in which a given number of molecules (typically 800-2000) were equilibrated at constant temperature. The simulation box for this stage had periodic boundary condition in the x and z directions, but was confined in the y direction by walls with a 9-3 LJ potential. The x and z box dimensions were designed to match those of the zeolite crystal in the (100) and (001) directions. The spacing between the LJ walls was adjusted to give a desired gas density. After equilibrium was reached, we began the second stage of the simulation, where the LJ walls were removed and the gas was placed alongside the zeolite with periodic boundary conditions in all directions. The gas molecules adsorbed onto the zeolite crystal and an equilibrium state point was reached when the pressure in the gas and the loading of the zeolite matched the adsorption isotherm for the system temperature. We show in Fig. 1 representative snapshots of one of our interface simulations. In Fig. 1(a) we show a side view of our simulation box, with the butane molecules in the gas, adsorption layer and zeolite colored red, yellow and light blue, respectively, and the zeolite represented by purple bonds. Fig. 1(a) shows a gas region with a pressure of approximately 5.5 MPa, and the corresponding highly loaded zeolite. In Fig. 1(b) we show a closeup snapshot of the adsorbed surface layer for the same system. Because we specify the system volume V, the number of molecules N, and the temperature T, the pressure P, and loading that are finally reached cannot be specified in advance, although with careful selection of N for a given T and V we can come close to any desired point on the isotherm.

The membrane permeation simulations were performed using the parallel grand-canonical (GC) MD code LADERA [45]. Two zeolite membranes were positioned in a simulation box of total length 137.30 Å, oriented so that the straight-channels traversed the membrane,

and the sinusoidal channels lay in the plane of the membrane. Each membrane had cross-sectional dimensions of 2 unit cells in the (001) direction and 3 units cells in the (100) direction (approximately 40 Å × 40 Å). The zeolite membranes separated the remaining volume into two gas regions, each approximately 29 Å thick. Periodic boundary conditions were applied in all three directions. Hence the simulation box represented an infinite set of infinite parallel zeolite membranes separated by gas regions of alternating high and low pressure. A constant chemical potential was maintained within a 15 Å thick region at the center of each gas region. This was done by performing insertions and deletions of gas molecules according to the GCMC algorithm [45]. Using this method, the pressures and densities on the high and low sides were maintained at constant but different values. At the same time, trajectories of all the molecules in the simulation box were followed using a conventional molecular dynamics algorithm, based on the LAMMPS code [27]. As a result, the simulation evolved in time to a condition of steady-state, with a constant net flux of molecules moving from the high-pressure side, through both zeolite membranes, to the low pressure side. This flux was maintained by a net addition of molecules in the high-pressure control volume and a net removal of molecules in the low pressure control volume.

For the permeation studies, the zeolite and gas molecule interaction potentials were identical to those described above, with two exceptions. First, the Lennard-Jones interactions were truncated at 10 Å but were not shifted. This has no effect on the permeation of molecules through the zeolite, which is only dependent on the forces, but it is important for the definition of chemical potential. Second, in the MD portion of the calculation, which used the velocity-Verlet algorithm with constant volume and temperature and a timestep of 3 fs, the temperature was controlled by velocity rescaling. We have found no difference when we ran the same state points with a Nosé-Hoover thermostat. A set of insertion and deletion attempts were performed in the control volumes every 1000 timesteps. Each set consisted of 32 attempts in each control volume, with insertions and deletions chosen at random with equal probability.

III. BULK PROPERTIES

Before discussing the dynamics of the gas–zeolite interfaces, we present our results for a bulk zeolite. These include the thermodynamic properties of zeolite adsorption as probed through adsorption isotherms, and diffusion studies in the infinite dilution limit and at finite loading.

A. Thermodynamic Properties

We begin with a comparison of the adsorption isotherms from both potential sets and experiment for both molecules. In Fig. 2(a) we show the comparison for *n*-butane with the mSKS and TraPPE force fields at 353 K with a cutoff of 10 Å . We have chosen these parameters to match those used in the MD simulations below. We also show in Fig. 2(a) the experimental data from Sun et al. [46] at the same temperature. The agreement is excellent for the TraPPE force field and fair for mSKS, but quite acceptable, considering that neither parameter set was optimized for adsorption studies.

We show the comparison for isobutane in Fig. 2(b). The agreement between TraPPE and mSKS is quite good, but neither force field can accurately reproduce the experimental data. In particular, both force fields fail to exhibit the plateau in the isotherm in the region of 4 molecules/unit cell, and overshoot the maximum filling by nearly a factor of two. This difficulty in fitting isobutane adsorption has also been seen by Macedonia and Maginn in their work with a constant-valence force field all-atom method [22]. That work found better agreement with a UA method with parameters that were optimized for zeolite adsorption. The lack of agreement between our calculated and experimental isotherms is a symptom of the origin of the force fields, and is a demonstration of the difficulty inherent in accurately treating the adsorption of complex branched molecules. We emphasize that our purpose in this section is to compare our state points with experiment, not to fit them. We are more interested in verifying that our MD interface simulations have converged to the correct state

points for a given model, and the isotherms shown in Fig. 2 serve that purpose.

In Fig. 3 (a) and (b) we show the GCMC isotherms for n-butane and isobutane, respectively, as a function of temperature. For comparison, we also show results from the MD interface runs at 500 K. We stress, however, that while isotherms can be successfully reproduced with the MD simulations, the direct integration of molecular trajectories leads to long equilibration times (in excess of 20 ns for isobutane), and thus extremely long run times. The GCMC method is much better suited to isotherm calculations, but is unable to give the dynamics of exchange that is the ultimate goal of this work.

The calculated isotherms can be fit well with a simple Langmuir isotherm,

$$q(P) = q_{sat}\frac{KP}{1+KP} \tag{4}$$

where $q(P)$ is the filling of the zeolite, q_{sat} is the saturation filling, P is the pressure, and K is the Langmuir constant. This has been shown previously by other authors [18]. We show these fits for 500K in Fig. 3(a) and (b). The good fits from the Langmuir isotherm suggest that the molecules have preferential adsorption sites within the zeolite. The Langmuir fits begin to fail at lower temperatures and higher pressures, due to the presence of additional adsorption sites that are relatively energetically unfavorable. For example, isobutane is known to preferentially load the intersections between the straight and sinusoidal channels in silicalite due to its large kinetic diameter [21]. At higher pressures, however, the intersections become filled, and the sorbed molecules are forced into the channels of the zeolite. Multiple adsorption sites can be taken into account by a double Langmuir fit, but we find this is not necessary for the majority of the pressures and temperatures we investigate here.

To conclude our thermodynamic studies, we investigate the effect of the LJ cutoff on the calculated isotherms. We perform the bulk of our simulations with a 10 Å cutoff, and show below that the effect of the cutoff on dynamic properties, such as the diffusivity at constant loading is small. The effect of the cutoff on the adsorption isotherms, however, is more severe. The TraPPE force field was originally parameterized using a 14 Å cutoff with the standard analytical tail corrections [32,33]. Tail corrections are applied with the implicit

assumption that the pair-pair correlation function attains a constant value of 1 beyond the cutoff, an assumption that is incorrect inside a zeolite, as demonstrated by Macedonia and Maginn [22]. The behavior of the model for infinite cutoff within a zeolite is therefore unknown. With this in mind, we present in Fig. 4 our GCMC isotherms for butane on silicalite as a function of the cutoff in the potential. The isotherms shift monotonically to higher fillings at a given pressure as the cutoff is increased. This is to be expected, since a larger cutoff leads to increased attractive energy. In the figure, the isotherms seem to be converging, though still changing, as the cutoff is increased from 14 Å to 18 Å. It is certainly possible to increase the cutoff until the isotherms converge, but such an exercise is beyond the scope of this work. Rather, we simply point out that the choice of cutoff is a model parameter that affects the calculated thermodynamic properties of any system. In Fig. 4, we also show the calculated isotherm with the TraPPE potential as published, i.e. with a 14 Å cutoff and tail corrections [32,33]. Even with the caveats above, this isotherm seems close to what would be expected for an infinite cutoff.

B. Diffusion Studies

With an understanding of the thermodynamics of sorption, we now move on to the behavior of the molecules within the zeolite. We begin with the calculated diffusion constant D in the infinite dilution limit. For all our diffusion measurements, we find the mean squared displacement of individual molecules, and calculate the diffusion constant based on the Einstein relation,

$$\langle r^2 \rangle = 6Dt \tag{5}$$

where $\langle r^2 \rangle$ is the mean squared displacement and t is the time. In Fig. 5 we show the calculated diffusivities over the temperature range of 400 K to 800 K for both butane and isobutane with the mSKS and TraPPE potential sets. The results for butane show that over the given temperature range the two potential sets perform identically. This result

is not surprising given that the parameterization for butane is almost unchanged between the two force fields. Both parameterizations calculate similar activation energies, 1.01 and 0.78 Kcal/mol for the mSKS and TraPPE potentials, respectively. These values compare well with experimentally measured activation energies for butane in silicalite, which range from $1-3$ Kcal/mol [13,12,47,14].

For isobutane, there is a substantial difference in the calculated diffusivities for the two parameter sets at all T. This difference is clearly due to the different treatment of the CH UA in the two parameter sets. In the mSKS parameterization, the CH UA has a radius $\sigma = 3.85$ Å and well-depth $\epsilon = 6.4 \times 10^{-2}$ Kcal/mol, while in the TraPPE parameterization the values are $\sigma = 4.68$ Å and $\epsilon = 1.99 \times 10^{-2}$ Kcal/mol. While the difference in σ is perhaps at first the most surprising, and the size comparison between CH and CH_2 ($\sigma = 3.95$ Å) and CH_3 ($\sigma = 3.75$ Å) for the TraPPE potential is counter-intuitive, we feel that this is not the cause of the differing diffusivities in Fig. 5. In spite of the fact that σ is so large for the CH UA, the surrounding CH_3 UAs effectively shield the CH group from the zeolite atoms. Instead it is the value of ϵ, which is smaller by a factor of 3.2 in the TraPPE potential that leads to the higher diffusivity. A smaller well depth necessarily implies less attraction to the walls of the zeolite, and it is this attraction that contributes most strongly to the diffusion constant in the infinite dilution limit. The weaker attraction is, of course, tempered somewhat by the larger value of σ, which implies more attraction at a longer distance. Both models do, however, give similar activation energies of 3.12 and 4.34 Kcal/mol for TraPPE and mSKS, respectively. These values also compare well with experimentally measured activation energies, which are generally around 5 Kcal/mol [13,47,14].

The good agreement with experimental activation energies is somewhat surprising, given that experiments cannot truly be performed at infinite dilution. With this in mind, we have also investigated the diffusivities of butane and isobutane at various loadings of the zeolite cages. In Fig. 6 we show the diffusion of butane in silicalite for both potential sets as a function of loading. Again it is clear that the small differences in the description of butane within the two force fields results in a minimal difference in the calculated diffusivity. In

Fig. 6 we also include experimental data taken from Heink et al. [11]. These data should not be taken as a strict comparison as they were not tabulated and were inferred from a figure. However, the agreement between simulation and experiment is still quite good.

Even better agreement between simulation and experiment in seen in Fig. 7 where we show the Arrhenius behavior of butane in silicalite at a fixed loading of eight molecules per unit cell. As we have found little difference between the mSKS and TraPPE potential sets, we will hereafter restrict our analyses to TraPPE, as it is designed to treat branched and linear molecules in a consistent fashion. The experimental data were again inferred from a figure in Heink et al. [11], but we still find excellent agreement between simulation and experiment. It is important to note, however, that in Fig. 6 the points for eight molecules per unit cell are already very close, and thus the excellent agreement in Fig. 7 is somewhat fortuitous. Had we chosen a different loading, while the activation energy would remain essentially unchanged, there would be a constant factor between the simulated and experimental diffusivities at all temperatures. Also shown in Fig. 7 is the calculated diffusivity at this loading and temperature with a cutoff of 14 Å. It is clear from the figure that the large cutoff has no effect on the diffusion constant at this loading. Since this loading is near to the maximum for butane in silicalite, the effect of the cutoff should be large here, and we can now fully justify our use of the smaller cutoff of 10 Å for our diffusion studies.

We conclude our study of diffusion in silicalite with Fig. 8 where we show the simulated and experimental diffusivity of isobutane at a variety of temperatures and loadings. The points for the simulations were chosen to coincide with the data, taken from Millot et al. [48], because of the difficulty in finding experimental diffusion studies of isobutane in a temperature range accessible to simulations. We show the temperatures and corresponding loadings for these data in Table II. The agreement here between simulation and experiment is fair, but we note two important points. First, the error bars on the experiment are quite large (a factor of three), which can greatly affect the slope of the line in the figure. Second, the experimental data here are from macroscopic membrane experiments, which are well known to disagree with MD simulations by an order of magnitude or more. With these

TABLE II. Temperatures and corresponding loadings for the diffusion data in Fig. 8.

Temperature (K)	Loading (molecules /unit cell)
398	3.5
473	2.5
573	1.0
673	0.5

points in mind, the agreement is quite acceptable.

IV. INTERFACE STUDIES

A. State Points

While relative diffusion rates and bulk sorption studies are of interest in separations applications, the tendency of a given species to adsorb preferentially over other species will also play an important role. As an example, we point to the permeation studies of Krishna and van den Broeke [49]. This work has shown that for binary mixtures of methane and butane, the flux is characterized by an initial sharp peak of methane, which quickly dies out and is replaced by a larger steady flux of butane. The authors ascribe the initial methane flux to its higher relative diffusivity. The relative adsorption, however, eventually leads to a higher filling of butane over methane, and then a higher butane output flux. From a practical standpoint, the adsorption properties must be understood first for pure component gases before the inherently more complicated behavior of mixtures is investigated. We discuss here the results of our interface studies for pure gases only, and will present our simulations of mixtures in a future paper [50].

Though most of the experiments on separations are at or near room temperature, we often found it necessary to work at more elevated temperatures. Accurate interpretations

of the dynamics of exchange between the gas and the zeolite require statistics gathered over a large number of actual exchange events. This in turn places requirements on the possible densities, and thus pressures, of the gas phase of the simulations. For good statistics, we need to run our simulations at gas pressures on the order of 100 kPa. Lower pressures imply extremely dilute gas regions, while higher pressures lead to fully loaded zeolites. Both these situations make exchange events rare. Pressures around 100 kPa then restrict us to high temperatures. At the lower temperatures often used in the experiments, pressures close to this would result in the zeolite being loaded to capacity and a thick wetting layer on the crystal surface. We expect (and find) the effects of such a dense adsorption layer on the exchange dynamics to be large and instead perform our simulations at state points where such effects do not exist. In addition, the higher temperatures lead to enhanced diffusivities of the sorbed species, which greatly reduces the computation burden. This is especially significant in the case of isobutane, which takes millions of time steps just to equilibrate, even at 500 K.

We show the state points of our MD simulations in Fig. 9, where we also show the vapor liquid coexistence curve (VLCC) for the TraPPE potential with a 10 $\mathring{A}$ cut and shifted potential. The VLCC for this potential set deviates considerably from the curve for the full TraPPE potential [32], which shows excellent agreement with experiment. The purpose of this figure, however, is not to compare to experiment, but rather to indicate the state points at which our simulations are performed. As is clear from the figure, we have focused on two different systems, a dilute system, which remains to the left of the coexistence curve at nearly all temperatures studied, and a dense system, which undergoes a phase separation as the temperature is lowered below the critical point T_c. In the figure it can be seen that the density of the adsorption layer of the dense system does not exactly match the liquid densities of the VLCC below T_c. This is primarily due to the definition of the adsorption layer, which is somewhat arbitrary. Small variations in this definition can lead to changes in the reported liquid densities in Fig. 9. The density of the adsorption layer of the dilute system does not lie on the VLCC curve because our MD simulations are performed at constant number of

particles. When phase separation occurs, the liquid layers formed may be unable to achieve the density that would be reached were an infinite particle bath available. For this reason, we will not include phase separated state points in the bulk of our discussions below.

B. Simulation Results

There are many different paths available for probing the dynamics of the exchanges between the gas and the zeolite. For example, one could choose to examine the mean adsorption time of molecules in the zeolite, or the mean time required for a gas molecule to become adsorbed. As these times can essentially be deduced from the diffusivities of the molecules, we have decided not to investigate these properties. Rather, we have chosen to investigate the relationship of the adsorbed surface layer to the exchanges. Our question is posed as follows: given a molecule which is in the gas at time t_0, leaves the gas at time t_g, and enters the zeolite at some time $t_z \geq t_g$, what is the mean time this molecule spends in the adsorption layer for times $t_g \leq t \leq t_z$? Furthermore, what are the variables that affect this mean time?

To begin, we show in Fig. 10 a center of mass density profile typical of our equilibrated interface simulations for butane. In this figure, the gas region extends from 80 Å to 184 Å, where the pressure is approximately 1.2 MPa. The small peaks of the adsorption layer can be seen near 82 Å and 182 Å, and are approximately 5 Å thick. The butane molecules can be seen to preferentially load the sinusoidal channels of the zeolite, as reported by other authors [21]. The smaller peaks in the zeolite portion of the density profile correspond to the straight channels, which become populated by butane as the gas pressure increases.

A molecule is identified as residing in the gas at some time t_g when its center of mass lies outside the zeolite and the adsorption layer [51]. Adsorbed molecules are identified by a similar criterion. As discussed below, the actual thickness of the adsorption layer is not strictly defined, and can affect results quantitatively, though not qualitatively. Consider the case shown in Fig. 11. The path shown by the dashed line represents a common trajectory in

which a molecule rapidly exchanges between the gas and the adsorption layer before settling into the layer and later entering the zeolite, represented by the solid line z. If the adsorption layer is chosen to be at dotted line 1, this molecule would be counted as spending a long time, t_1 in the adsorption layer. However, if the adsorption layer were chosen to be at either dotted line 2 or 3, the exchanges would not be counted, and the value of t_{ads} would be a much smaller time, t_2 or t_3.

In Fig. 12, we show the distribution of time spent in the adsorption layer, t_{ads}, by molecules entering the zeolite from the gas for the dilute and dense system, representing a pressure range of approximately 1-20 MPa at $T = 500$ K. Note the distribution in the figure is dramatically different from the overall lifetime of molecules in the adsorption layer, which has an exponential form as shown in the inset. From Fig. 12, it is clear that ballistic entry makes up only a small part of the exchange events. A rough calculation indicates that a molecule entering the zeolite ballistically should spend approximately 1 ps in the adsorption layer at 500 K. The resolution in Fig. 12 is 2 ps, implying that ballistic entry events will be divided between $t = 0$ ps and $t = 2$ ps bins. It is clear from the figure that the bulk of the molecules spend substantially longer than 1 ps in the adsorption layer, and the mean time is, in fact, on the order of 20 ps. It is also clear from the figure that the pressure dependence, and therefore the dependence on zeolite loading, is extremely weak, at least for the pressure range shown in the figure. The distribution for $N(t_{ads})$ is normalized so that the integral under the curve gives the number of molecules entering the zeolite per timestep.

We have fit the distribution for t_{ads} shown in Fig. 12 with a simple binomial distribution of the form

$$P_{n,p}(\nu) = \begin{pmatrix} n \\ \nu \end{pmatrix} p^{\nu}(1-p)^{n-\nu} \tag{6}$$

where P is the total probability, p is the probability of success in a single trial, n is the number of trials, and ν is the number of successes [52]. For the particular case here, we are only interested in the first entry into the zeolite, i.e. one success, giving $\nu = 1$. The number of trials, n, is equal to a constant times t for a random walker physisorbed to the zeolite

surface, and we then fit to the probability of success in a single trial. Eq. 6 then reduces to

$$P_{t,p} = Ap(t/\tau)(1-p)^{t/\tau-1} \tag{7}$$

where we have included an arbitrary multiplicative constant A to account for normalization factors, as well as a normalization factor τ to keep the exponent dimensionless. In Fig. 12 we also show the fits from Eq. 7. For these data, the timestep was reduced to 1.25 fs with molecular configurations saved every 0.5 ps in order to increase the resolution. As can be seen in the figure, the fits are quite good for a value of $p = 0.33$. The fits are most accurate at small t_{ads}, but begin to underestimate the data at longer times. This effect is primarily due to our choice of the width of the adsorption layer. The choice of the layer width can have a strong effect on the distributions shown in Fig. 12, as shown in Fig. 11. However, as this choice is somewhat subjective, rather than attempt to explain the slight differences between the fits and the data, we point out that the fits demonstrate a physically reasonable functional form for the lifetimes.

A binomial distribution suggests that there are a number of distinct adsorption sites on the (010) surface of the zeolite, and adsorbed molecules quickly jump from site to site until they either enter the zeolite or return to the gas. We have examined the validity of this conclusion by calculating the density profile of the physisorbed molecules, shown in Fig. 13(a) and (b) for butane and isobutane, respectively. For these figures, we show a contour plot of the density of physisorbed molecules averaged over the entire production phase of the simulation, with white (black) representing regions of high (low) density. For clarity we only show a subsection of the total system in the figures. In the figures, it can be seen that there are a number of distinct adsorption sites surrounding the pore mouths that are preferentially occupied by the butane and isobutane molecules. The highest density is seen to be directly over the pore mouth, indicating that the molecules do not snake their way into the zeolite, hugging close to the surface, but rather hop directly into the potential well of the pore mouth. This picture is consistent with Burggraaf [53], who showed that when the ratio of the kinetic diameter of the sorbed molecules to the pore opening is close to 1,

as is the case for butane in silicalite, sorbed molecules feel a deep potential well inside the pores, with nearly equal contributions from both walls. It is interesting to note that the distributions for butane and isobutane are identical.

In addition to t_{ads} for molecules entering the zeolite, we have investigated the related distribution for molecules that leave the zeolite and enter the gas. In Fig. 14 we show the distribution for t_{ads} for $T = 500K$ and $P = 1200kPa$ for molecules entering the zeolite from the gas (i.e. the same distribution shown in Fig. 12) as well as that for molecules leaving the zeolite and entering the gas. The two distributions are identical within statistical error, indicating that ballistic transport is, again, a relatively unfavorable process. This result also suggests that there are different desorption points for molecules entering the gas and the zeolite. As discussed above, from Fig. 13 it is clear that molecules entering the zeolite do so by first hopping to an adsorption site directly above a pore mouth. Molecules leaving the zeolite and entering the adsorption layer must first exit a pore via this same site. If this site were also the site for desorption into the gas, then the probability for ballistic exit (or very small t_{ads}) in Fig. 14 would dominate. This is not the case. Rather, molecules leaving the zeolite enter the adsorption layer via the adsorption site directly over the pore mouth, and then hop from adsorption site to adsorption site until the preferred site for desorption into the gas is reached. This, coupled with the lack of variation of t_{ads} over a wide pressure range, indicates that even for extremely low back-pressures, such as those realized in membrane permeation experiments with sweep gases, desorbing and adsorbing molecules will feel the same resistance to transport into or out of the zeolite.

In Fig. 15 we show the mean value of t_{ads} for our dilute and dense systems as a function of temperature. For the resons discussed above, we do not show the mean times for the dense sytem below T_c in the figure. From the figure it is clear that the mean time is nearly insensitive to pressure at all temperatures, and shows a weak temperature dependence. The effect of temperature on the mean shows that entry into the zeolite is an activated process related to surface diffusion. The insensitivity to pressure implies that identical surface barriers exist on both sides of membranes in permeation simulations and experiments. Also

shown in the figure are representative points for isobutane molecules entering the zeolite. It is an interesting and unexpected result that the mean time is nearly identical for butane and isobutane.

A distinct difference between the dilute and dense system exists in the orientation of surface adsorbed molecules. The angular orientation of the adsorbed molecules can be found by finding the distribution of the angles between the end-to-end vector of all adsorbed molecules and the (010) surface of the zeolite. In order to remove artifacts caused by the finite width of the adsorption layer, we show the differences between angular distributions, rather than the individual distributions themselves. The effect of the width should be the same for all distributions, and should thus cancel out for the differences.

In Fig. 16 we show the difference in angular distribution between the dilute and dense systems for two different temperatures, 500 K and 200 K. Although 200 K is well below T_c for the dense system, we have chosen to show this temperature because the effect on the angular distribution becomes more pronounced at lower temperatures. Additionally, although the liquid densities of systems at these low temperatures may not reach the same level as systems coupled to an infinite particle bath, these effects should be more pronounced at the vapor/liquid interface, while the vapor/solid interface (represented here by the first adsorption layer) should not be strongly affected. In the figure it is clear that at 500 K, where both systems are supercritical fluids, there is little difference in the angular distributions. At 200 K, however, there is a strong difference. Because the figure shows the dense system distribution subtracted from the dilute system distribution, an excess in the former (latter) will be realized as a negative (positive) peak. At 200 K, physisorbed molecules in the dilute system tend to lie flat on the surface. Such a conformation is allowed because of the low density of physisorbed molecules, and preferred because it maximizes their energy of adsorption. In the dense system at 200 K, the adsorption layer become so densely packed that the molecules must begin to stand on end. This change in angular distribution can also be seen in Fig. 17, where we show the distributions at 200 K subtracted from those at 500 K for both systems. Again, it is clear that molecules in the dilute system lie down on the surface

at low temperatures, while those in the dense system tend to stick out. We predict that the orientation of the molecules in the dense system will actually lead to shorter mean times when compared to the dilute system at lower temperatures. This is because in the dense system, molecules are already in the preferential position to enter the zeolite, and simply need to find a pore mouth, whereas in the dilute system, the molecules must additionally lift themselves off the surface, losing adorption energy, in order to enter a pore. We have performed a similar analysis for isobutane, using the angle between the plane formed by the three CH_3 UAs and the surface of the zeolite. However, we have not found any appreciable difference in the distributions as a function of temperature or density for the systems we studied.

V. PERMEATION STUDIES

We performed simulations for pure butane and pure isobutane at temperatures of 400K and 500K and several different pressure drops. Each simulation consisted of a series of consecutive runs, lasting from 10 to 20 ns. The first run in each simulation began either with an empty system, or used the final configuration from a previous simulation. During each run, the density profile across the membrane and the flux across the membrane were measured. The flux was calculated from the average of the net number of molecules added on the high-pressure side and the net number of molecules deleted on the low-pressure side, divided by the membrane area and the duration of the run. Once all of these quantities stopped changing from one run to the next, steady-state was assumed to have been reached, and the results from the final run were used. The time required to reach steady-state ranged from 10 to 100 ns.

The pressures in the upstream and downstream gas phases were calculated from the gas phase densities. On the low-pressure side, this was done using the ideal gas law. On the high-pressure side, we used pressure-volume isotherms obtained by direct isobaric-isothermal Monte Carlo simulation of the bulk gas. The permeability Π was calculated using the

following equation:

$$\Pi = \frac{J}{\Delta P/L}$$

where J is the flux rate of molecules across the membrane, ΔP is the difference between the upstream and downstream gas pressures, and L is the membrane thickness (40 Å). In all cases, the downstream pressure was much smaller than the upstream pressure, so the pressure-drop and upstream pressure were almost equal in magnitude. The variation of n-butane and isobutane permeability with pressure-drop and temperature is shown in Fig. 18. In all cases, we see the same general behavior. For low pressure drops, the permeability is independent of the pressure. As the pressure drop increases, the permeabilities start to decrease strongly. Both of these behaviors are correctly captured by the simple permeation model based on the Langmuir isotherm. The constant permeability at low pressure corresponds to the Henry's law regime, where loading increases linearly with pressure. At sufficiently high pressures, excluded volume interactions cause the isotherm to flatten out, resulting in a monotonically decreasing permeability.

As a comparison, we also show in Fig. 18 the theoretical permeabilities as a function of pressure for butane and isobutane at the simulation temperatures. Following Burggraaf [53], we have calculated the permeability based on our Langmuir isotherm fits from section III A, and diffusivities from section III B. The theoretical flux is given as

$$J = q_{sat}\frac{D_c}{L}ln(\frac{1+KP_f}{1+KP_m}) \tag{8}$$

where D_c is the transport diffusivity and P_f (P_m) is the pressure on the feed (membrane) side. Following Maginn et al. [54], we have used the self-diffusivity in the infinite dilution limit as a value for D_c. As can be seen in the figure, the theoretically predicted permeabilities are consistently an order of magnitude greater than those from the simulation. Actual experimental measurements of butane and isobutane permeation at low pressure drops show permeabilities of about 10^{-10} and $10^{-11}(mol/m^2/s)/(Pa/m)$, respectively [55], and agree well with the theoretical results.

One reason for this underprediction can be inferred from the density profiles obtained from the simulations. For example, Fig. 19 shows the profiles for n-butane at 500K for both high and low pressure drops . Each membrane exhibits four density peaks corresponding to the locations of the channel intersections where most of the open space in the zeolite is located. The outer peaks are slightly lower than inner peaks due to the lower number of zeolite atoms interacting with the n-butane molecules that are near the surface. What is striking about the profile is the perfect symmetry within each membrane i.e. there is no concentration gradient. This indicates that the molecules within the zeolite are at equilibrium. This implies that the flux rate is limited by processes other than diffusion through the interior of the zeolite. Possible limiting processes include diffusion on the upstream surface of the zeolite or activated escape from the last zeolite cavity out into the low-pressure gas. The same absence of gradient is seen in all the n-butane runs.

Fig. 20 shows the corresponding profiles for isobutane. In this case, we do see the formation of a concentration gradient in the direction of flow, and this is also true for the other isobutane simulations. It appears that switching from n-butane to isobutane results in a decrease in the relative importance of the surface resistance.

The absence of internal density gradients has also been observed by Pohl and Heffelfinger [56], and more recently by Nitta *et al.* [57] The presence of surface barriers could be viewed as an anomaly associated with the extremely thin membrane sample which we have used. In fact, it could explain why our permeability predictions lie far below the experimental range. One might expect that as the membrane thickness is increased, surface effects will become negligible. However, it is not clear if this is true for the zeolite particles used in typical membranes.

VI. CONCLUSIONS

We have presented the results of molecular dynamics simulations of interfaces between single component gases of butane and isobutane and silicalite. We have investigated the

dynamics of exchange between the gas and the zeolite. In particular, we have found that molecules from the gas enter the zeolite primarily via the adsorption layer, where they hop among preferred adsorption sites until entering a pore mouth. Molecules desorbing from the zeolite undergo a similar process in reverse. For both processes, t_{ads} is found to be on the order of 20 ps, and is unchanged over a wide range of gas pressures, and only weakly affected by system temperature. The dominant effect is found to be the surface coverage of the adsorption layer of the zeolite. The small variance of t_{ads} with change in state point leads to significant transport resistance at both the feed and permeate sides of membrane permeation experiments and simulations, and is the most likely cause of the discrepancy between the simulation results and theoretical permeations based on Langmuir isotherms.

Future work will investigate the preferential adsorption of binary gas mixtures and its role in separations processes.

ACKNOWLEDGMENTS

We thank Tina Nenoff for many useful discussions. We thanks Scott Sides for insightful discussions, assistance with the nonlinear fitting, and the generation of graphics. We also thank Mike Macedonia and Ed Maginn for their initial calculations of butane isotherms with the TraPPE potential. Sandia is a multiprogram laboratory operated by Sandia Corporation, a Lockheed Martin Company, for the United States Department of Energy under Contract DE-AC04-94AL85000.

FIG. 1. (a) Snapshot of an interface simulation at 500 K. Butane molecules in the gas, adsorption layer and zeolite are red, yellow, and light blue, respectively, while the zeolite is represented by purple bonds. The density of the adsorption layer and the filling of the zeolite can be clearly seen. (b) Close up view of the adsorption layer from Fig. 1 (a).

FIG. 2. Adsorption isotherms for (a) butane and (b) isobutane in silicalite at 353 K. Experimental data from Sun *et al.* is shown as a solid line. Simulation results are shown for TraPPE with a 10 Å cut and shift (diamonds) and mSKS with a 10 Å cut and shift (squares).

REFERENCES

[1] W. M. Meier and D. H. Olson, *Atlas of Zeolite Structure Types* (Butterworth-Heinemann, London, 1992).

[2] D. Schuring, A. P. J. Jansen, and R. A. van Santen, J. Phys. Chem. B **104**, 941 (2000).

[3] E. B. Webb III, G. S. Grest, and M. Mondello, J. Phys. Chem. B **103**, 4949 (1999).

[4] A. Corma, C. R. A. Catlow, and G. Sastre, J. Phys. Chem. B **102**, 7085 (1998).

[5] A. Bouyermaouen and A. Bellemans, J. Chem. Phys. **108**, 2170 (1998).

[6] R. C. Runnebaum and E. J. Maginn, J. Phys. Chem. B **101**, 6394 (1997).

[7] W. J. M. van Well *et al.*, J. Phys. Chem. B **102**, 3945 (1998).

[8] H. Jobic, M. Bee, and G. J. Kearley, Zeolites **146**, 146 (1992).

[9] H. Jobic, M. Bee, and G. J. Kearley, Zeolites **9**, 312 (1989).

FIG. 3. Adsorption isotherms for (a) *n*-butane and (b) isobutane in silicalite as a function of temperature. Simulation results using TraPPE 10 Å cut and shift are shown at 400 K (circles), 500 K (squares), and 600 K (diamonds). The data are connected with lines as a guide to the eye, except for the case of 500 K, where the lines are fits from a Langmuir isotherm. For *n*-butane, the simulation results calculated at 500 K using the MD interface code are shown as stars. Experimental data is not available at these temperatures.

FIG. 4. Adsorption isotherms for n-butane in silicalite at 500 K as a function of the cutoff. Simulation results are shown for the TraPPE force field with a potential truncation of 10 Å cut and shift (circles), 14 Å cut and shift (diamonds), 18 Å cut and shift (squares), and 14 Å with tail corrections (crosses). Simulation results are connected by lines as a guide to the eye.

FIG. 5. Diffusion constant D of butane and isobutane as a function of temperature in silicalite in the infinite dilution limit. Open (closed) circles refer to the mSKS (TraPPE) potential set for butane, while open (closed) triangles refer to the same potential sets for isobutane.

[10] J. Caro *et al.*, J. Chem. Soc., Faraday Trans. 1 **81**, 2541 (1985).

[11] W. Heink *et al.*, J. Chem. Soc., Faraday Trans. **88**, 3505 (1992).

[12] O. P. Keipert and M. Baerns, Chem. Eng. Science **53**, 3623 (1998).

[13] A. S. Chiang, A. G. Dixon, and Y. H. Ma, Chem. Eng. Science **39**, 1461 (1984).

[14] A. Paravar and D. T. Hayhurst, 6^{th} P. Int. Zeol. C. 217 (1984).

[15] M. P. Allen and D. J. Tildesley, *Computer Simulation of Liquids* (Clarendon, Oxford, 1987).

[16] W. Liang, S. Chen, and S. Peng, Ind. Eng. Chem. Res. **36**, 1882 (1997).

[17] S. C. Reyes, J. H. Sinfelt, and G. J. DeMartin, J. Phys. Chem. B **104**, 5750 (2000).

[18] W. Zhu *et al.*, Ind. Eng. Chem. Res. **37**, 1934 (1998).

[19] E. J. Maginn, A. T. Bell, and D. N. Theodorou, J. Phys. Chem. **99**, 2057 (1995).

[20] B. Smit and T. L. Maesen, Nature **374**, 42 (1995).

[21] T. J. H. Vlugt *et al.*, J. Am. Chem. Soc. **120**, 5599 (1998).

[22] M. D. Macedoina and E. J. Maginn, Mol. Phys. **96**, 1375 (1999).

[23] C. J. Mundy, J. I. Siepmann, and M. L. Klein, J. Chem. Phys. **102**, 3376 (1994).

[24] M. Tuckerman, B. J. Berne, and G. J. Martyna, J. Chem. Phys. **97**, 1990 (1992).

[25] M. Mondello and G. S. Grest, J. Chem. Phys. **103**, 7156 (1995).

[26] E. B. Webb III and G. S. Grest, Catalysis Letters **56**, 95 (1998).

[27] S. Plimpton, J. Comp. Phys. **117**, 1 (1995).

[28] J. I. Siepmann, S. Karaborni, and B. Smit, Nature **365**, 330 (1993).

[29] B. Smit, S. Karaborni, and J. I. Siepmann, J. Chem. Phys. **102**, 2126 (1995).

[30] J. I. Siepmann, M. G. Martin, C. J. Mundy, and M. L. Klein, Mol. Phys. **90**, 687 (1997).

[31] B. Smit, S. Karaborni, and J. I. Siepmann, J. Chem. Phys. **109**, 352 (1998).

[32] M. G. Martin and J. I. Siepmann, J. Phys. Chem. B **102**, 2569 (1998).

[33] M. G. Martin and J. I. Siepmann, J. Phys. Chem. B **103**, 4508 (1999).

[34] Molecular Simulations Inc., San Diego, CA.

[35] R. L. June, A. T. Bell, and D. N. Theodorou, J. Phys. Chem. **96**, 1051 (1992).

[36] G. C. A. M. Mooij, D. Frenkel, and B. Smit, J. Phys. Condens. Matter **4**, L255 (1992).

[37] M. Laso, J. J. de Pablo, and U. W. Suter, J. Chem. Phys. **97**, 2817 (1992).

[38] J. I. Siepmann, Mol. Phys. **70**, 1145 (1990).

[39] J. I. Siepmann and D. Frenkel, Mol. Phys. **75**, 59 (1992).

[40] D. Frenkel, G. C. A. M. Mooij, and B. Smit, J. Phys. Condens. Matter **4**, 3053 (1992).

[41] J. J. de Pablo, M. Laso, and U. W. Suter, J. Chem. Phys. **96**, 2395 (1992).

[42] A. Z. Panagiotopoulos, Mol. Phys. **61**, 813 (1987).

[43] A. Z. Panagiotopoulos, N. Quirke, M. Stapleton, and D. J. Tildesley, Mol. Phys. **63**, 527 (1998).

[44] B. Smit, P. de Smedt, and D. Frenkel, Mol. Phys. **68**, 931 (1989).

[45] A. P. Thompson, D. P. Ford, and G. S. Heffelfinger, J. Chem. Phys. **109**, 6406 (1998).

[46] M. Sun, D. B. Shah, H. H. Xu, and O. Talu, J. Phys. Chem. B **102**, 1466 (1998).

[47] J. Kärger and D. Ruthven, *Diffusion in Zeolites and Other Microporous Solids* (Wiley, New York, 1991).

[48] B. Millot *et al.*, J. Phys. Chem. B **103**, 1096 (99).

[49] R. Krishna and L. J. P. van den Broeke, Chem. Eng. J. **57**, 155 (1995).

[50] M. Chandross, E. B. Webb III, and G. S. Grest, (to be published).

[51] The true boundary between the gas region and the adsorption layer is open to interpretation, but as long as the bulk of the peaks seen in Fig. 10 are included, the results should not change greatly.

[52] We note that the data shown in Fig. 12 are all for simulations with a Langevin thermostat. We have duplicated the simulations with a Nosé-Hoover thermostat, and find that we can still fit the distributions to a binomial, but with different values of p, and thus different mean times spent in the adsorption layer.

[53] A. J. Burggraaf, J. Membr. Sci **155**, 45 (1999).

[54] E. J. Maginn, A. T. Bell, and D. N. Theodorou, J. Phys. Chem. **97**, 4173 (1993).

[55] F. Kapteijn, J. van de Graaf, and J. A. Moulijn, J. Mol. Catal. **134**, 201 (1998).

[56] P. I. Pohl, G. S. Heffelfinger, and D. M. Smith, Mol. Phys. **89**, 1725 (1996).

[57] T. Nitta and S. Furukawa, Mol. Sim. (to appear).

FIG. 6. Diffusion constant D as a function of loading for butane in silicalite at 400K. Simulated (experimental) points are represented by circles ('x's), and the open (filled) circles represent points calculated with the mSKS (TraPPE) force field. The experimental data is taken from Heink et al. [11].

FIG. 7. Diffusion constant D of butane in silicalite as a function of temperature at a finite loading of the zeolite cage (8 molecules/unit cell). Agreement between simulation data (filled circles) and experiment (crosses) are excellent. Also shown is the calculated diffusion at 400 K with a cutoff of 14 $\mathring{A}$ (open triangle). The change in cutoff has no effect on D.

FIG. 8. Diffusivities of isobutane in silicalite at various temperatures and loadings (see text). The temperatures and loadings were picked so that the simulated points (closed triangles) coincide with the experimentally available data (upside down triangles) [48].

FIG. 9. State points of the butane MD simulations. The density of the gas (adsorption layer) of the dilute system is shown as closed (open) circles, while that for the dense system is shown as closed (open) squares. The vapor liquid coexistence curve for this potential set is also shown as crosses with a dotted line to guide the eye.

FIG. 10. Typical density profile along the (010) crystal direction. The state point in the figure represents 800 butane molecules at 500 K, which leads to a gas pressure of 1.2 MPa and a loading of 7.3 molecules per unit cell. The two adsorption layers are centered at approximately $y = 82$ Å and $y = 182$ Å, and are approximately 5 Å thick.

FIG. 11. Schematic diagram of a molecule rapidly exchanging between the gas and adsorption layer before residing in the adsorption layer and entering the zeolite.

FIG. 12. Time spent in the adsorption layer by butane molecules as they enter the zeolite from the gas. The squares and circles represent $P = 1.2$ and $8.?MPa$, respectively, while the solid and dashed lines are fits of the low and high pressure points, respectively, to a binomial distribution as described in the text. The inset shows the overall lifetime of molecules in the adsortpion layer.

FIG. 13. Density profile of (a) butane and (b) isobutane molecules in the adsorption layer over the entire simulation at 500 K. The profile is overlayed over the bonds of the unit cell for clarity. There are a number of distinct adsorption sites present on the surface.

FIG. 14. A comparison of t_{ads} for butane molecules entering the zeolite from the gas (squares) and those entering the gas from the zeolite (circles). The data are for T=500 K and P = 1200 kPa, and are identical within statistical error.

FIG. 15. Mean time spent in the adsorption layer by butane molecules as a function of temperature. The times for the dense (dilute) system are shown as squares (circles). We do not show points below T_c for the dense system. Representative times for a dilute system of isobutane are shown as open squares.

FIG. 16. Difference between the angular distributions of the dense and dilute systems of butane molecules in the adsorption layer. Excess in the dilute (dense) system is shown as a positive (negative) peak. There is no difference at 500 K, while at 200 K molecules in the dilute (dense) system tend to lie on (stick up from) the surface.

FIG. 17. Differences in angular distributions as a function of temperature for butane molecules in the adsorption layer of the dilute and dense systems. Excess at 500 K (200 K) is shown as a positive (negative) peak. As the temperature changes from 500 K to 200 K, molecules in the dilute (dense) system tend to lie on (stick up from) the surface.

FIG. 18. Permeability of butane and isobutane through a silicalite membrane as a function of pressure drop and temperature. Butane and isobutane are shown as open and closed figures, respectively, while the circles and squares represent 500 K and 400 K, respectively. Also shown are the theoretical permeabilities for butane at 500 K (dashed line) and isobutane at 400 K (dotted line).

FIG. 19. Density profiles for butane permeating across a silicalite membrane with pressure-drops of 20,300 kPa and 491 kPa at $T = 500$K.

FIG. 20. Density profiles for isobutane permeating across a silicalite membrane with pressure-drops of 22,400 kPa and 535 kPa at $T = 500$K.

a)

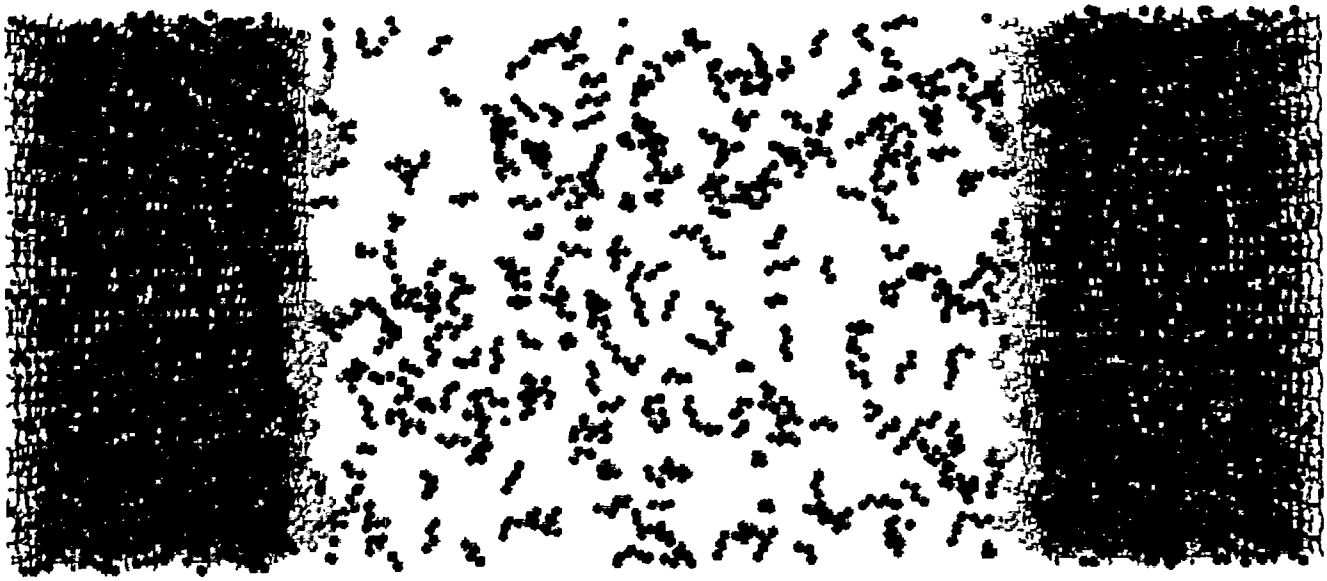

b)

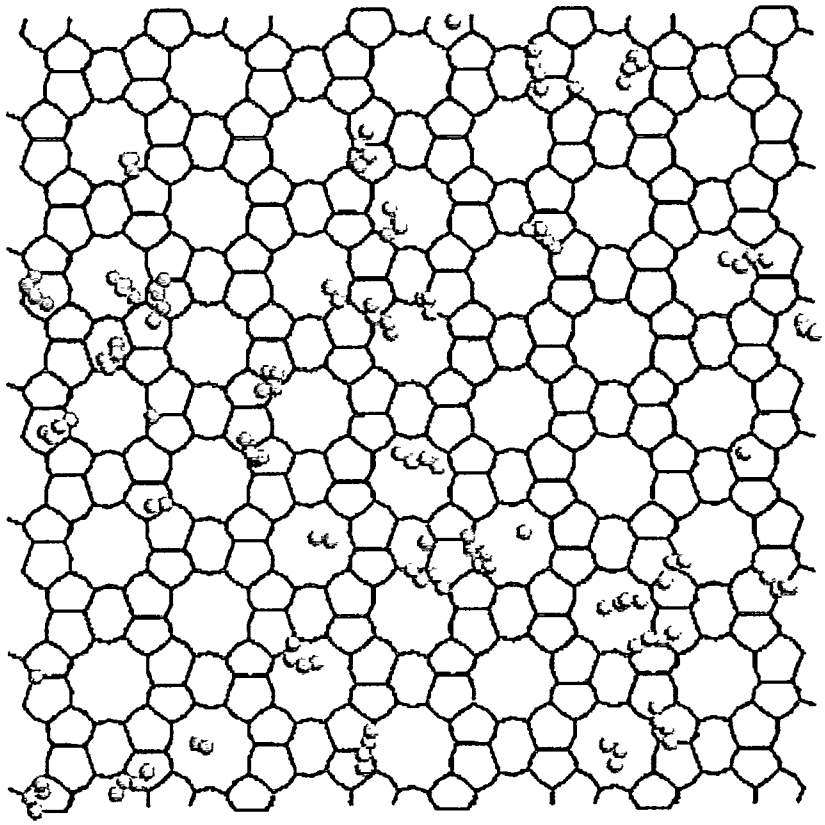

Chandross, etal., Fig. 1

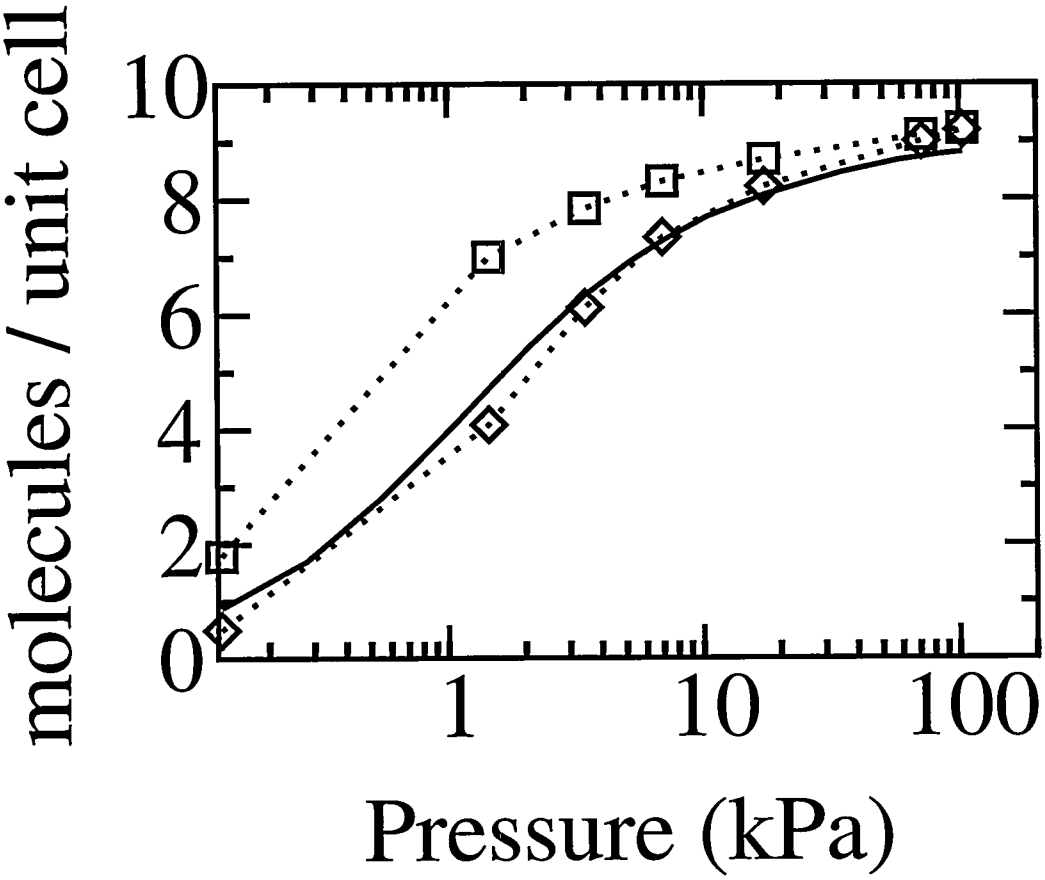

Chandross et al., Fig. 2a

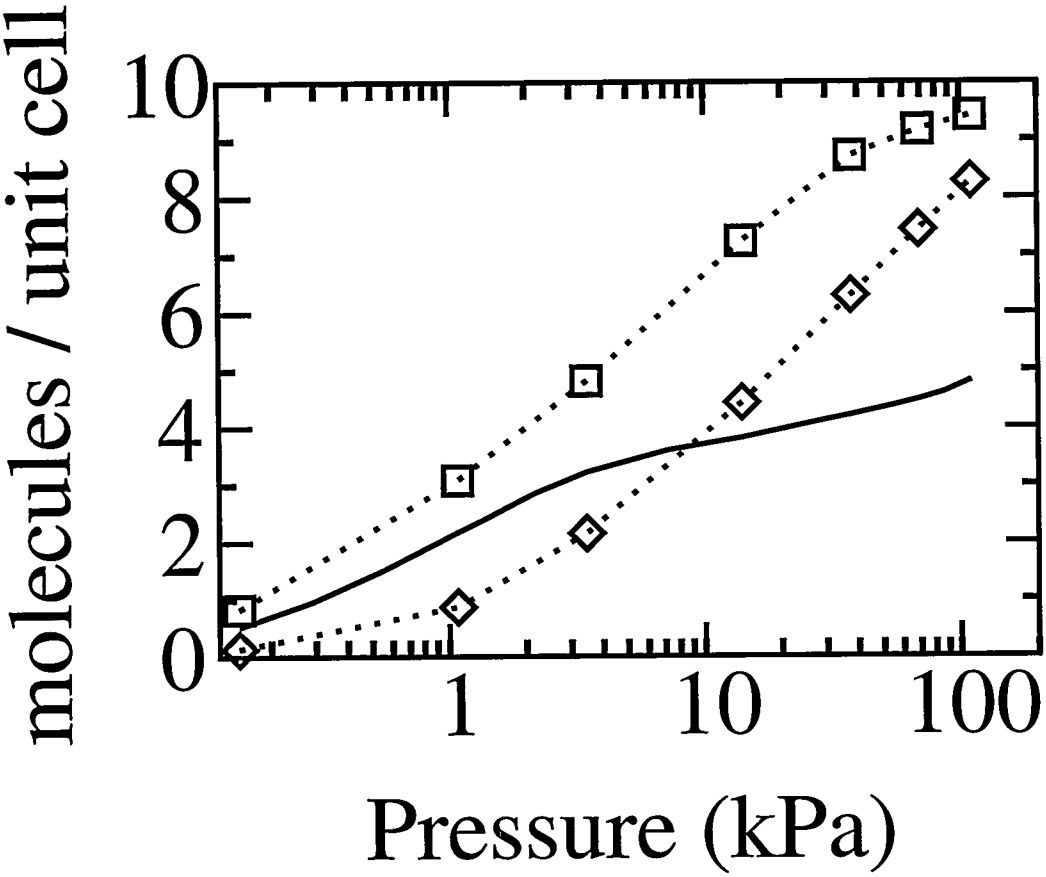

Chandross et al., Fig. 2b

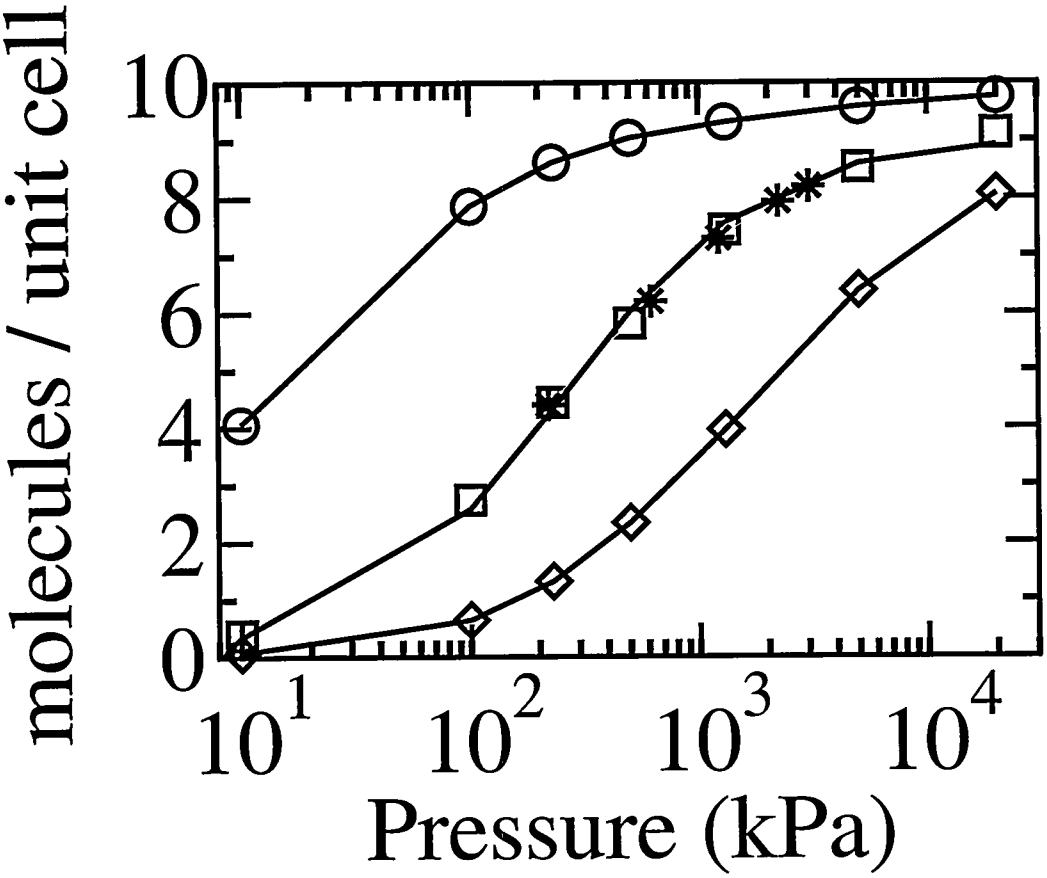

Chandross et al., Fig. 3a

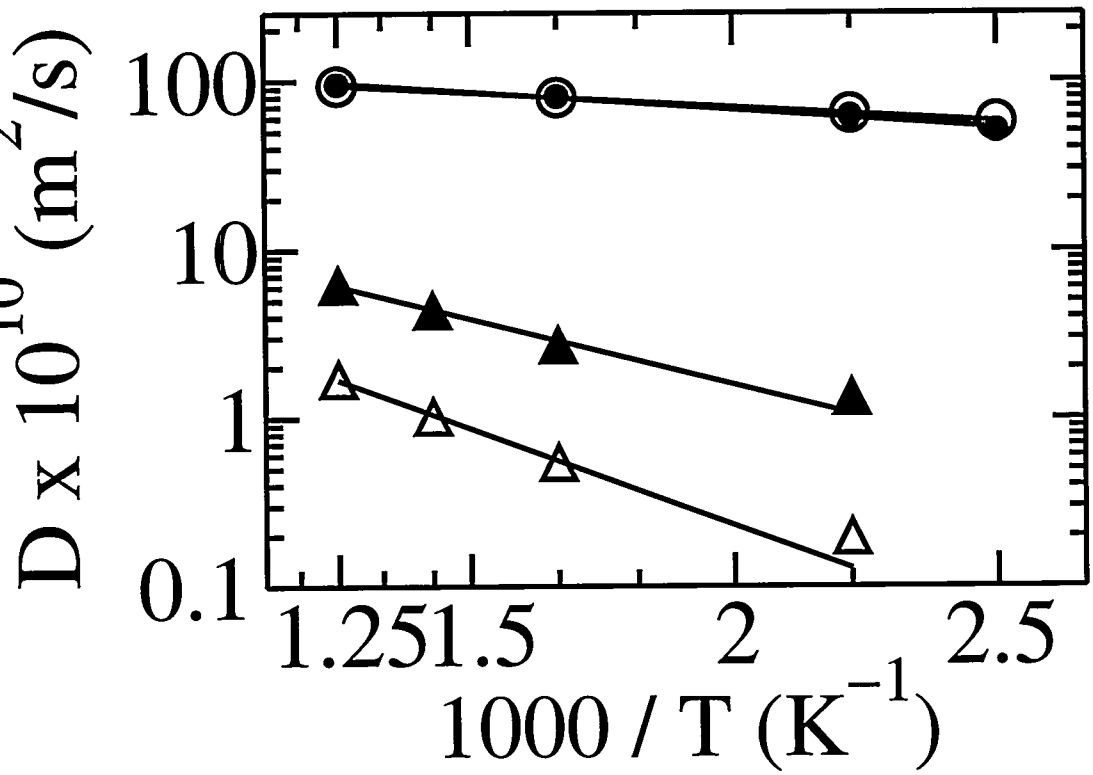

Chandross, et al., Fig. 5

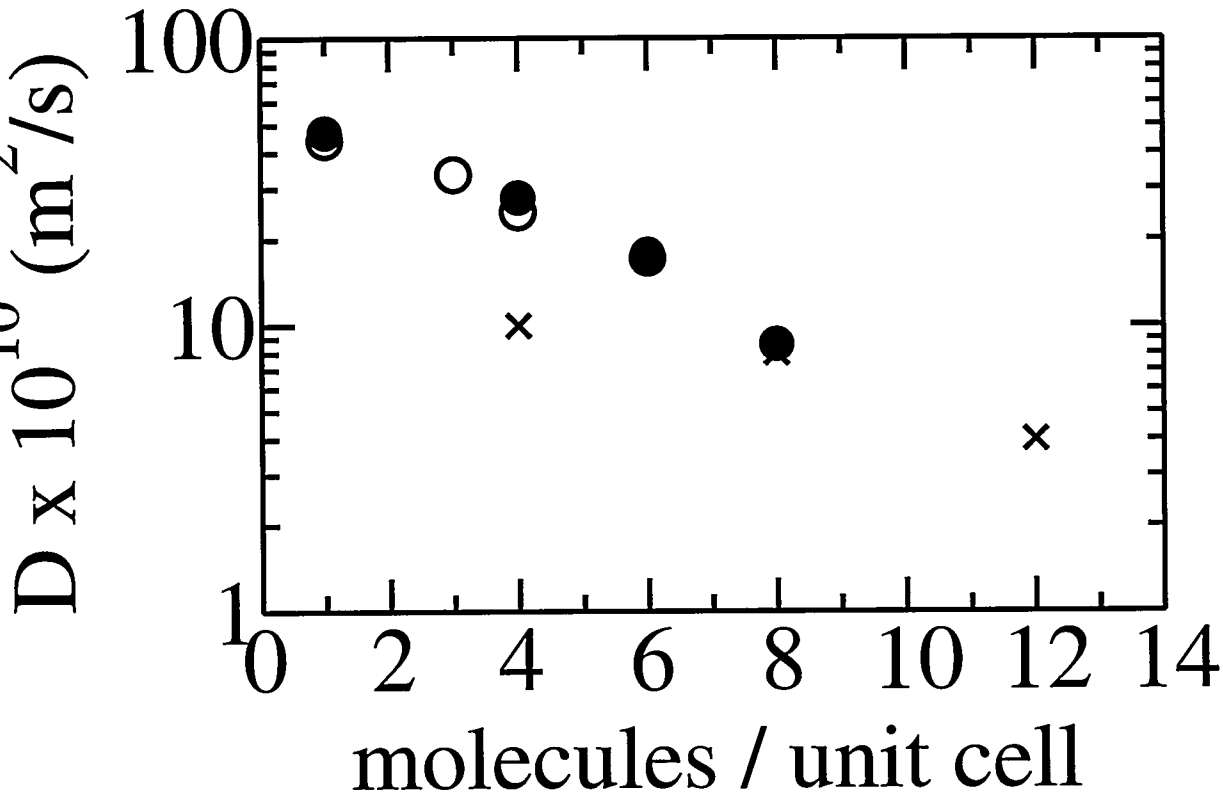

Chandross, et al., Fig. 6

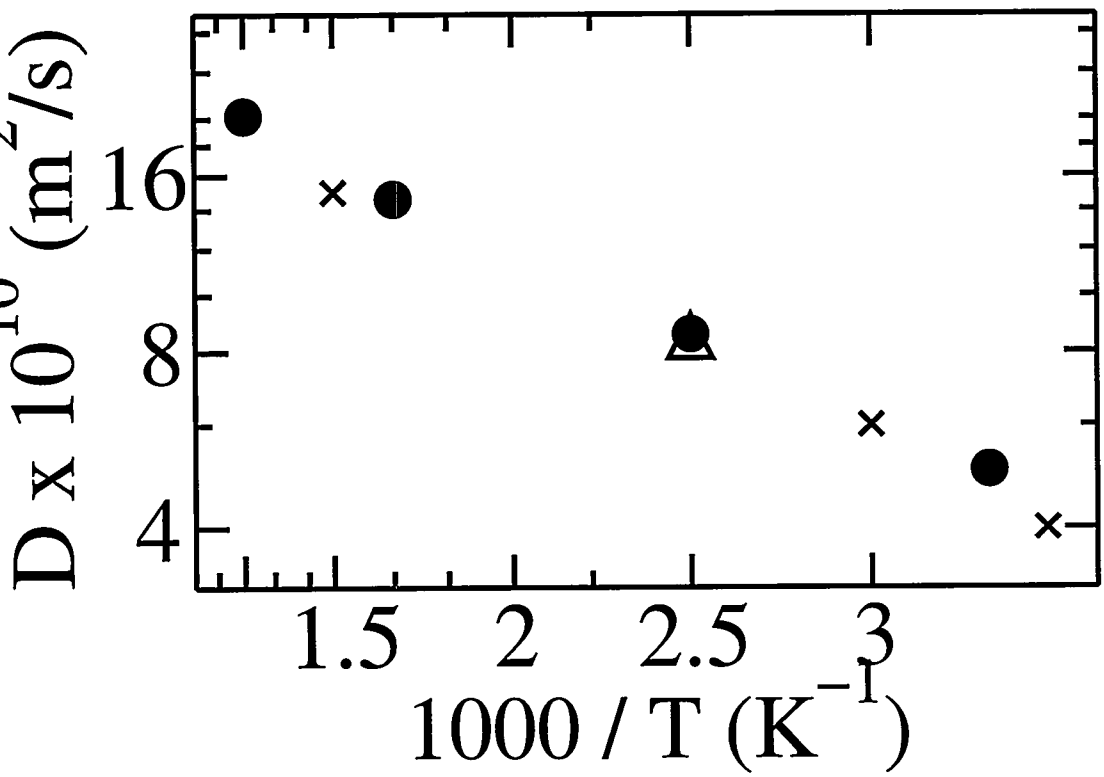

Chandross, et al., Fig. 7

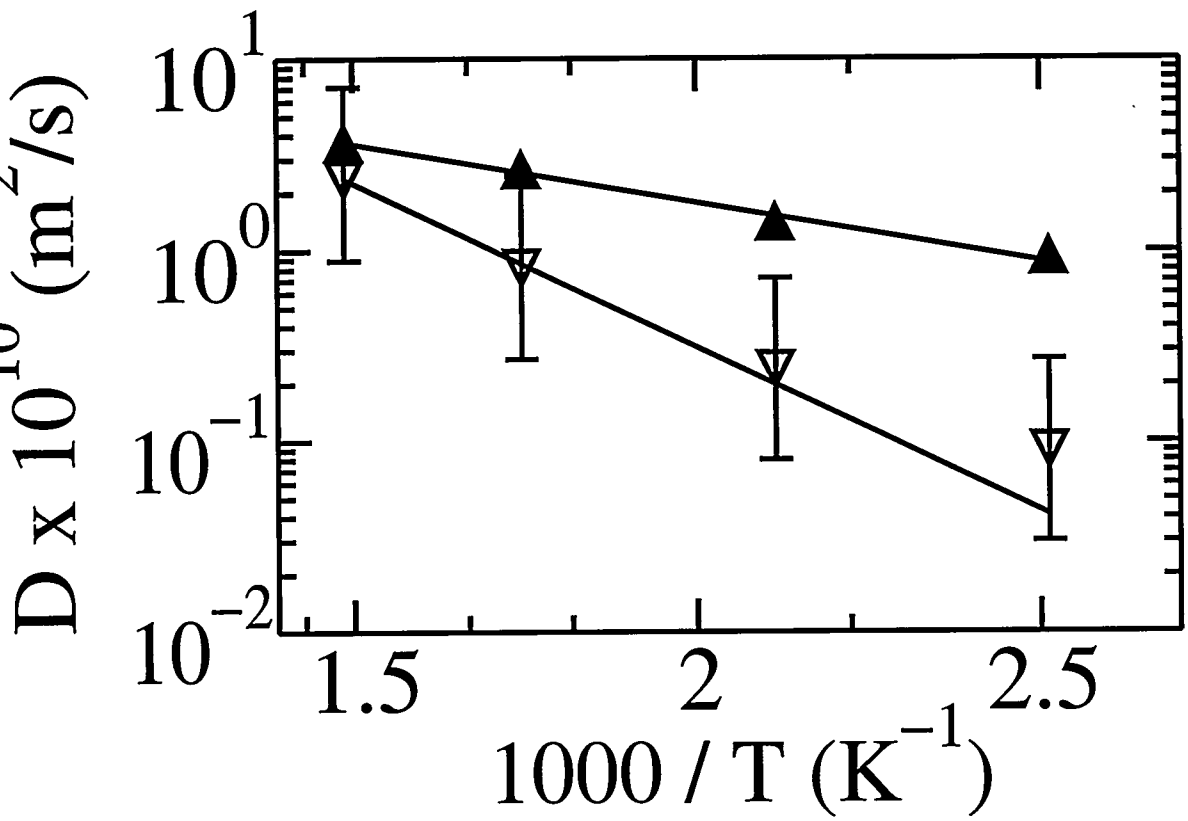

Chandross, et al., Fig. 8

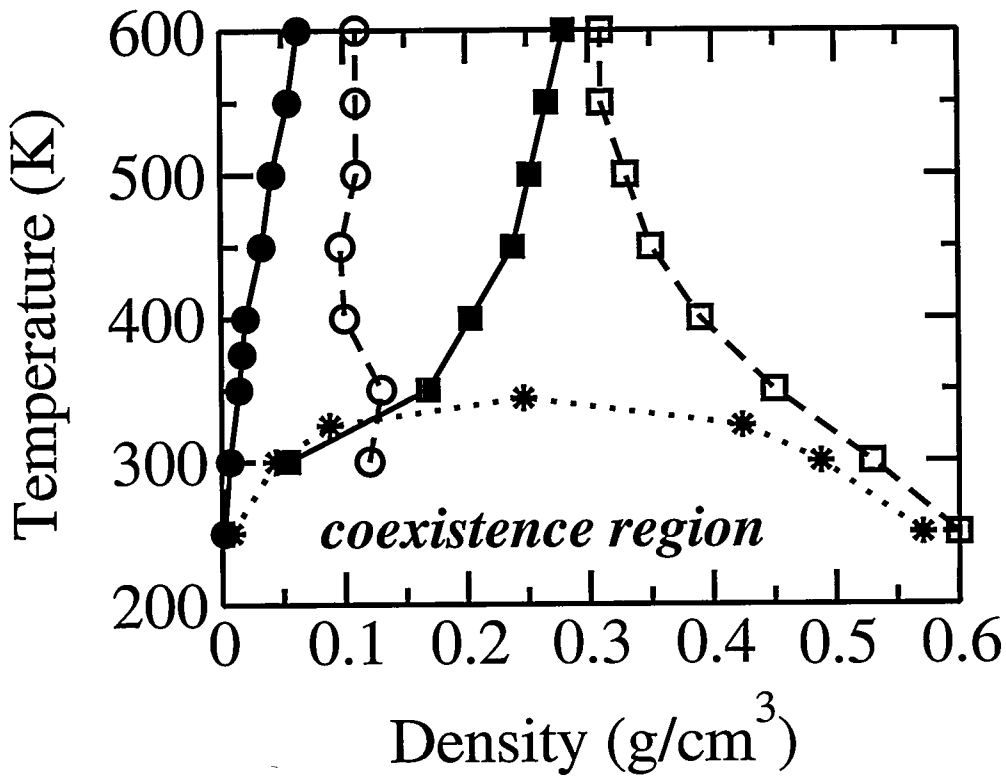

Chandross, et al., Fig. 9

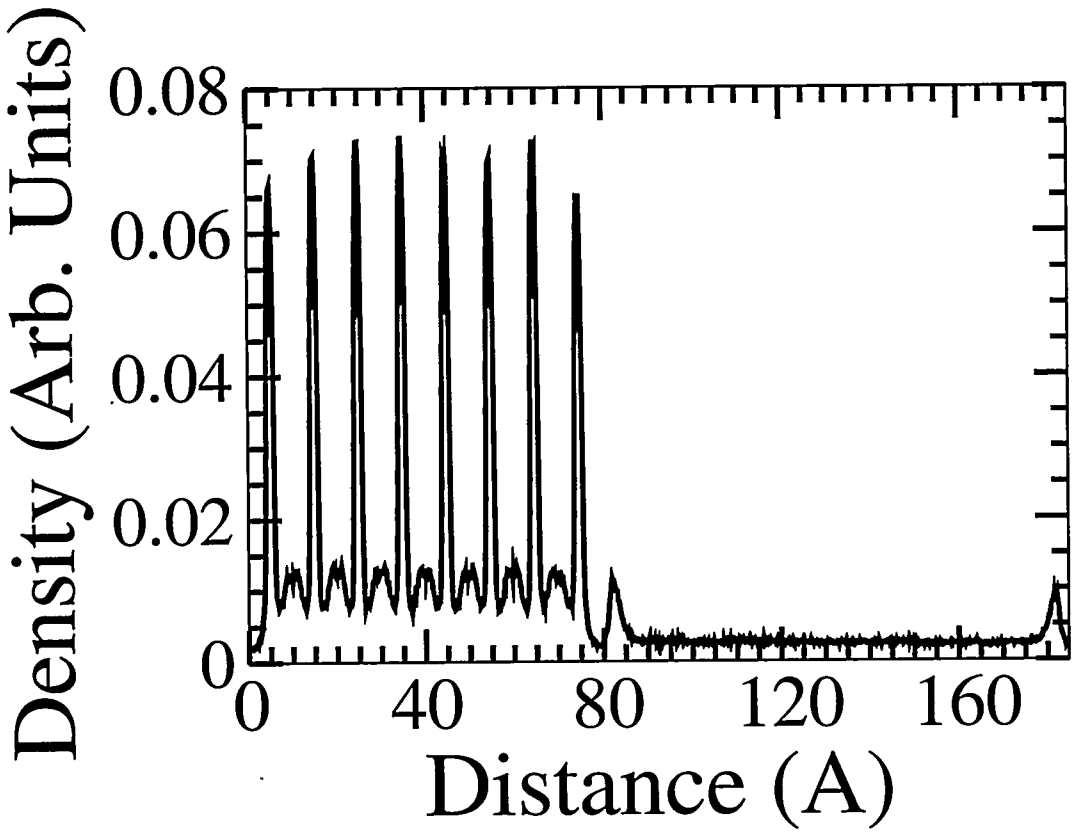

Chandross, et al., Fig. 10

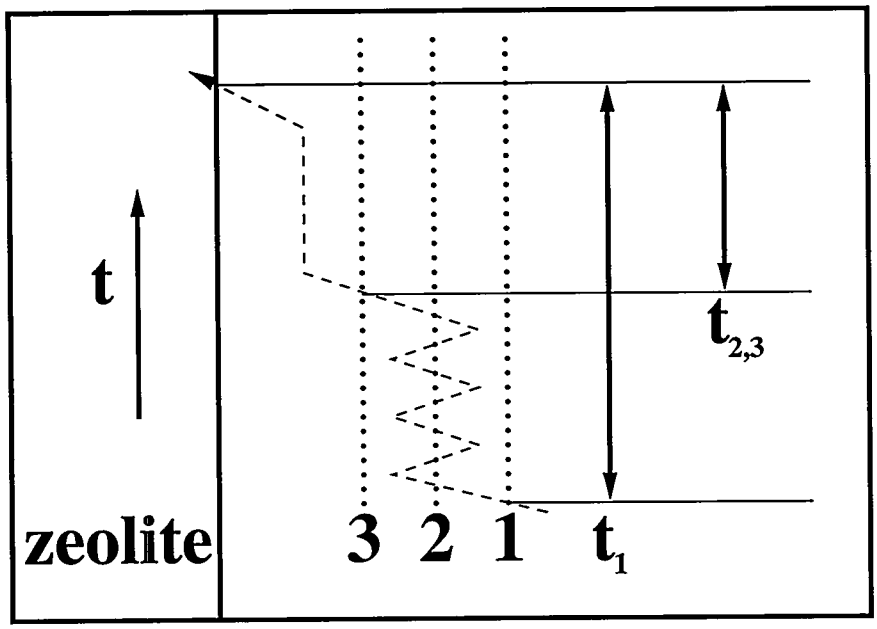

Chandross et al., Fig. 11

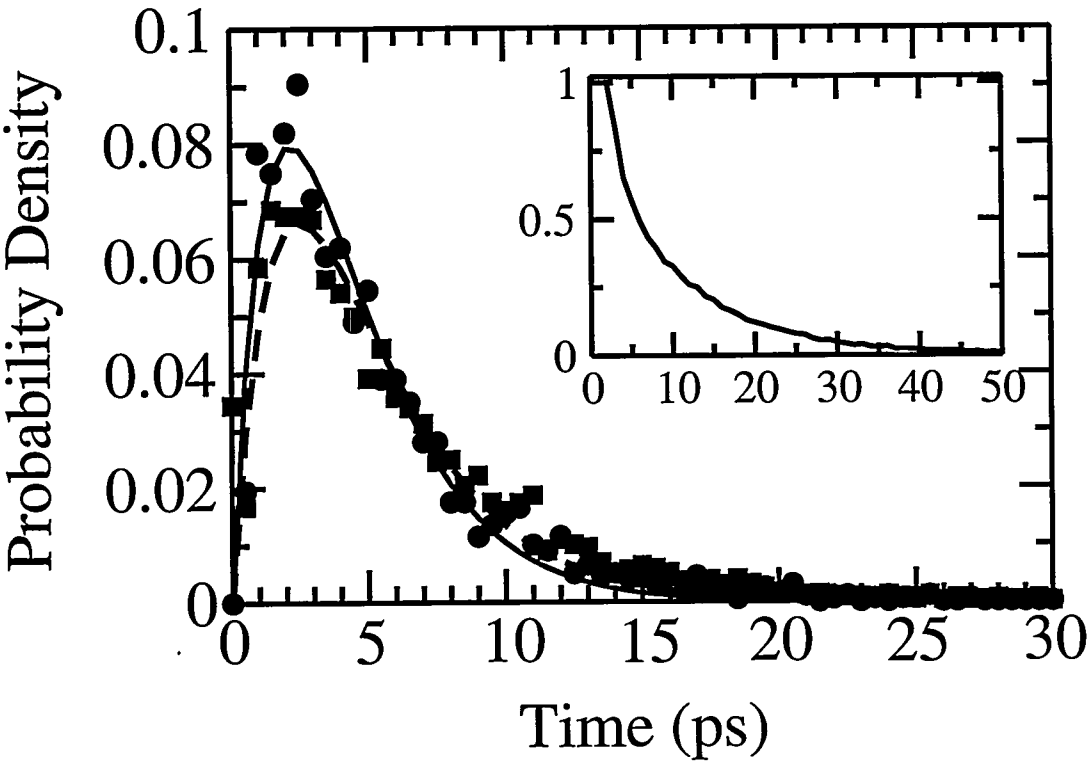

Chandross, et al., Fig. 12

Chandross, et al., Fig 13(a)

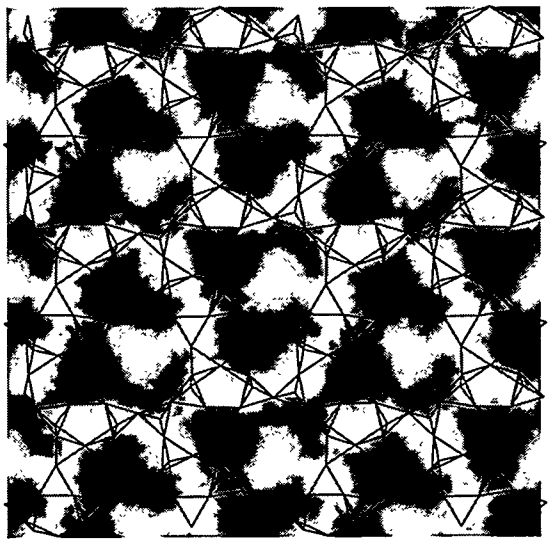

Chandross, et al., Fig 13(b)

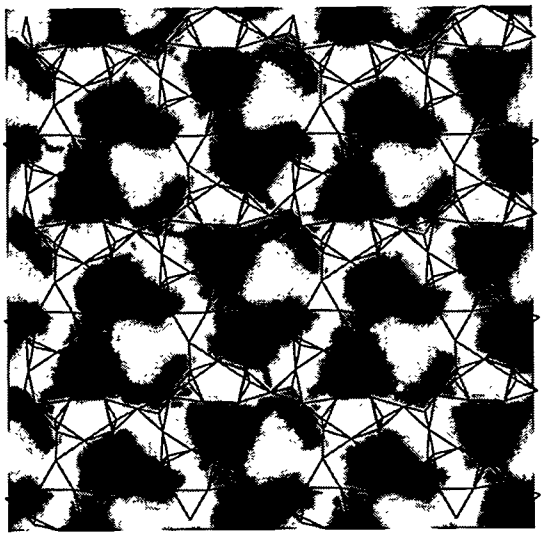

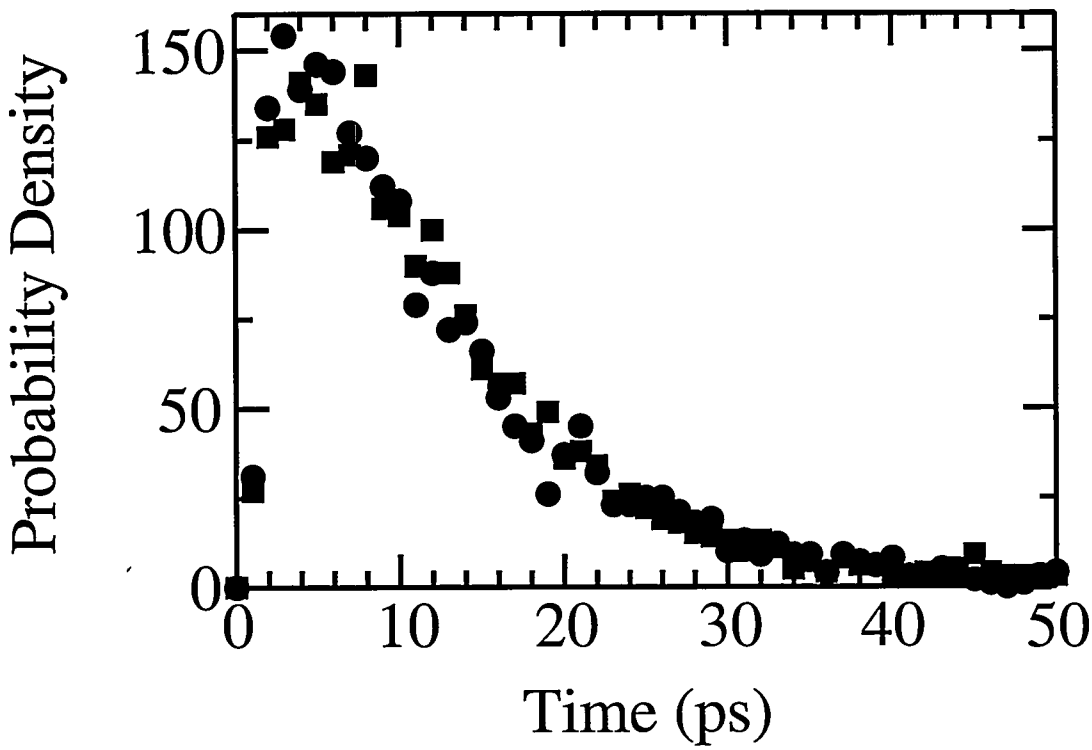

Chandross, et al., Fig. 14

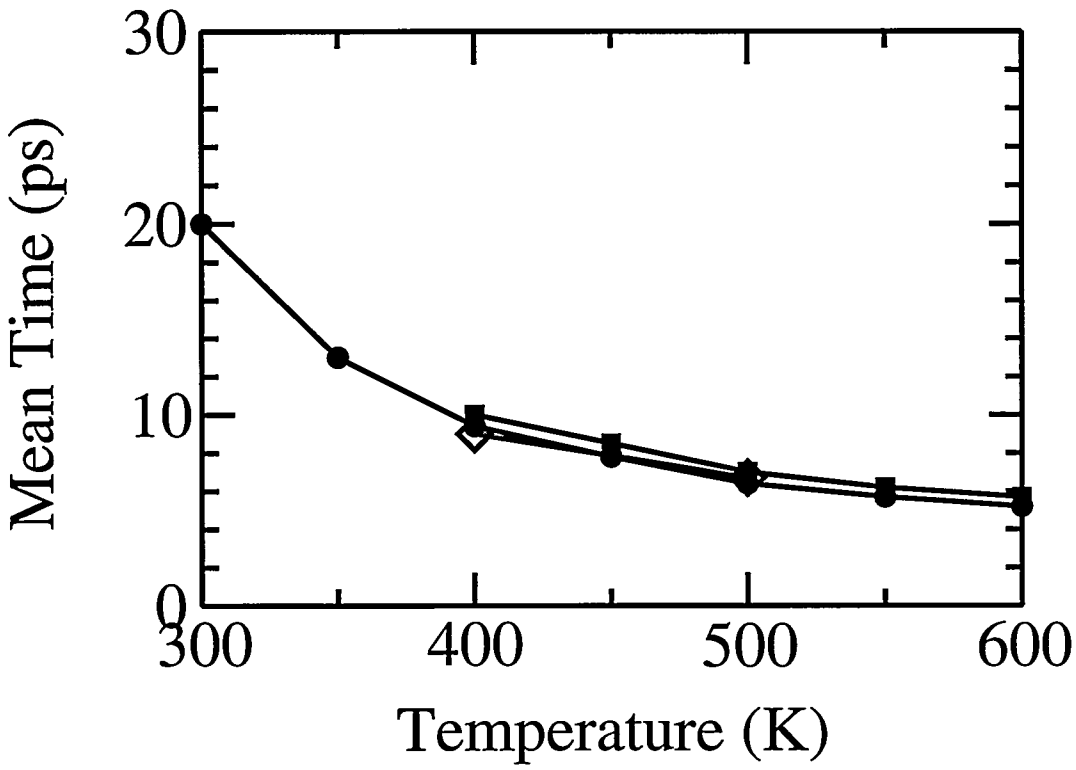

Chandross, et al., Fig. 15

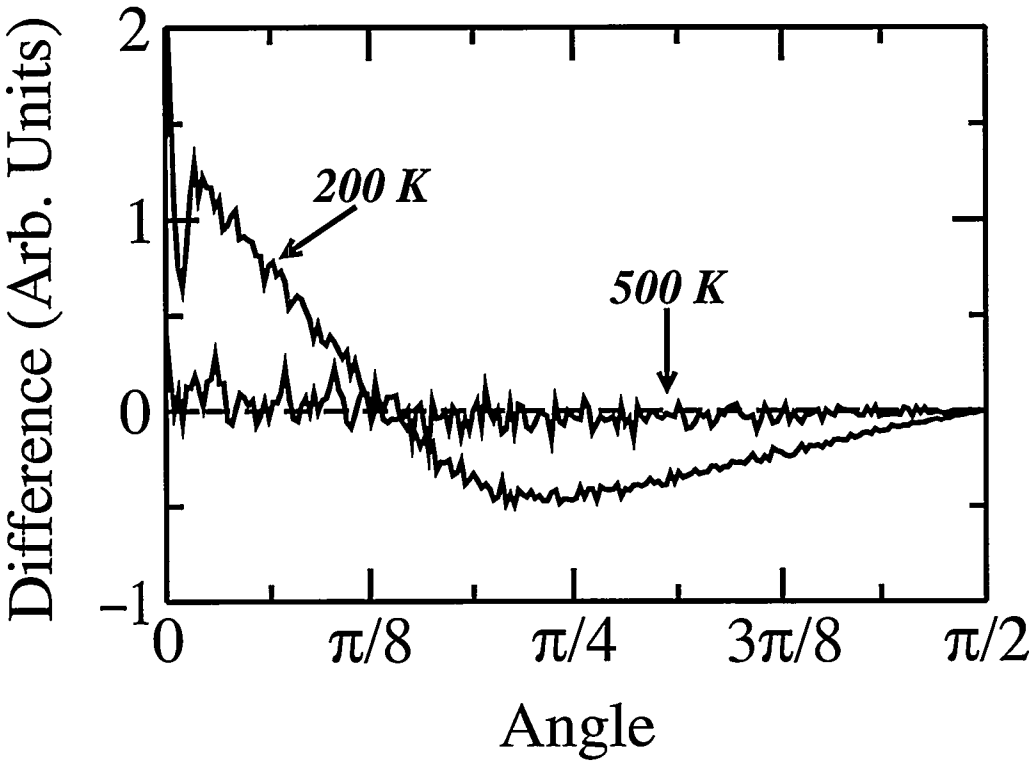

Chandross, et al., Fig. 16

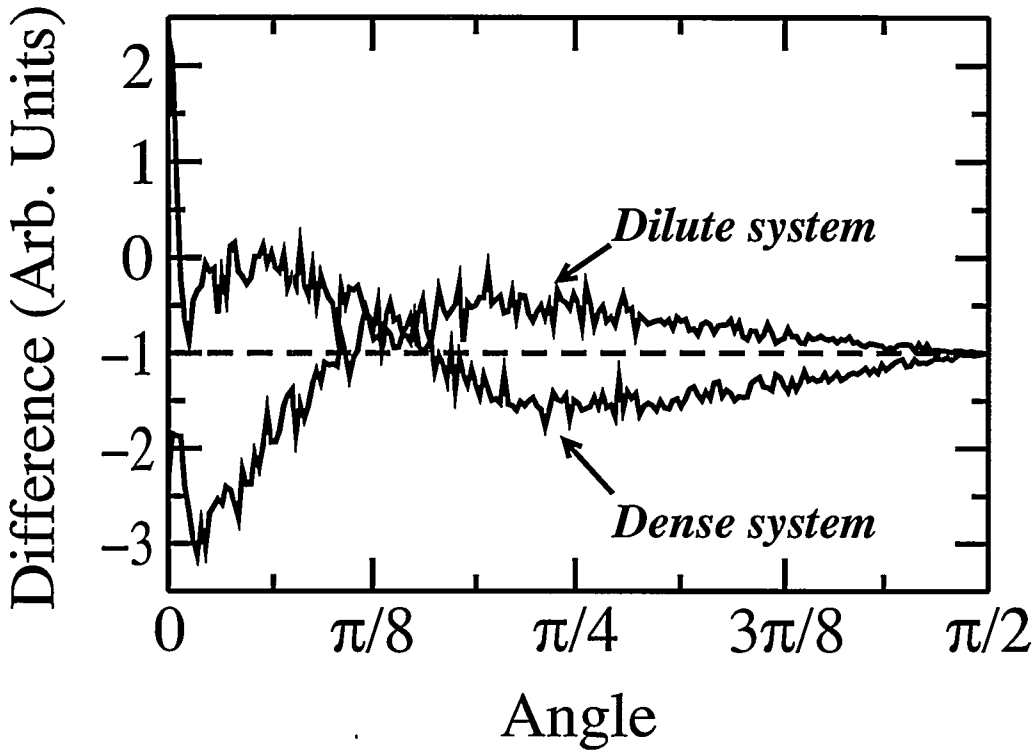

Chandross, et al., Fig. 17

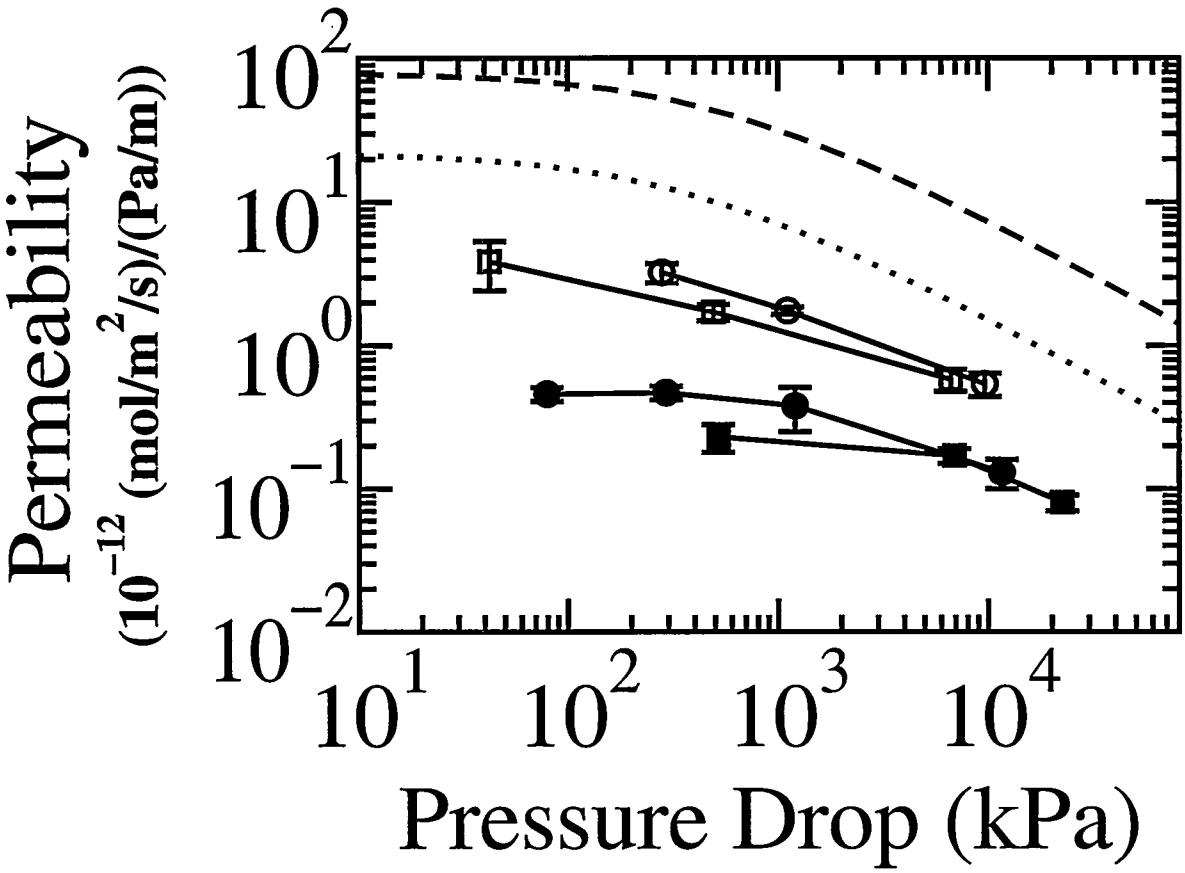

Chandross, et al., Fig. 18

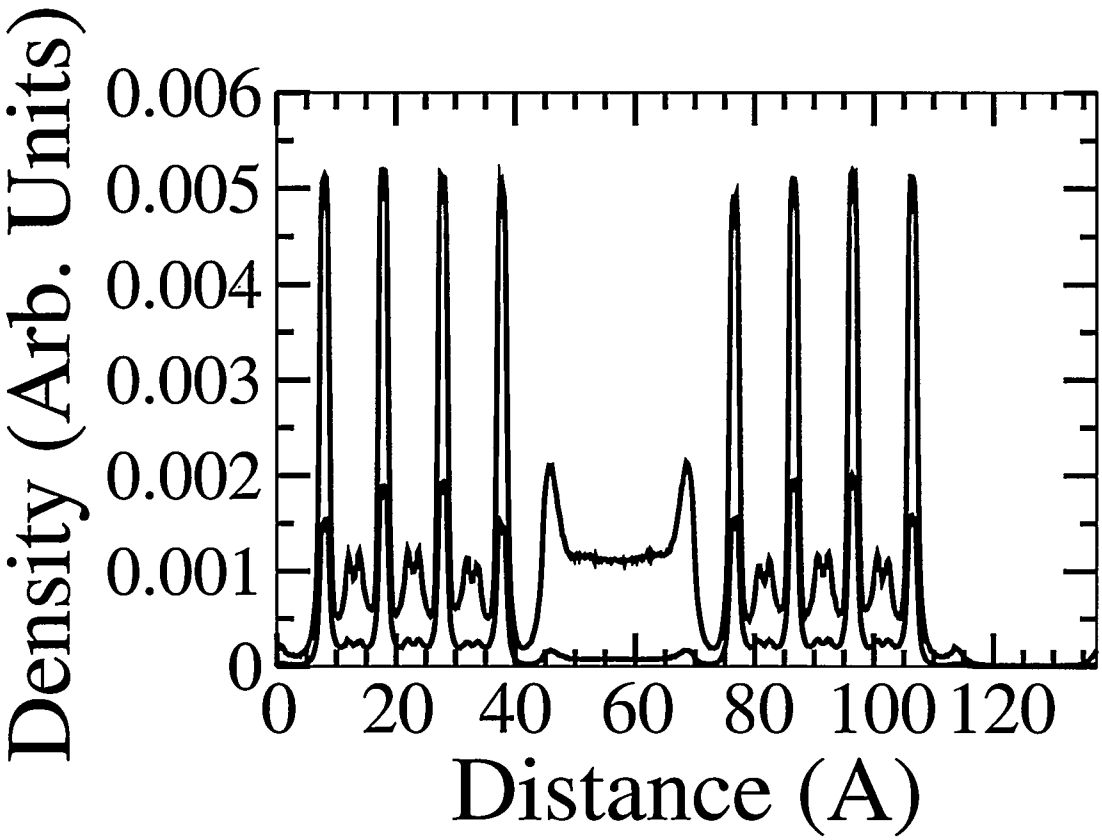

Chandross, et al., Fig. 19

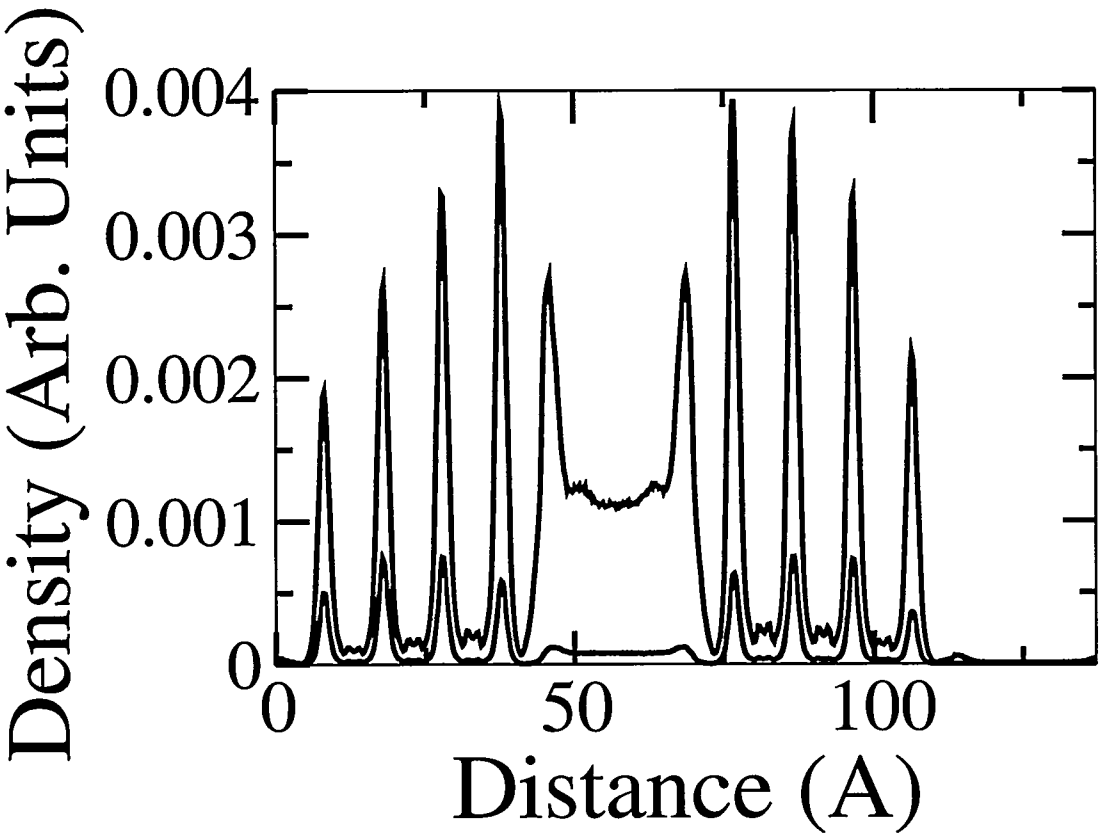

Chandross, et al., Fig. 20

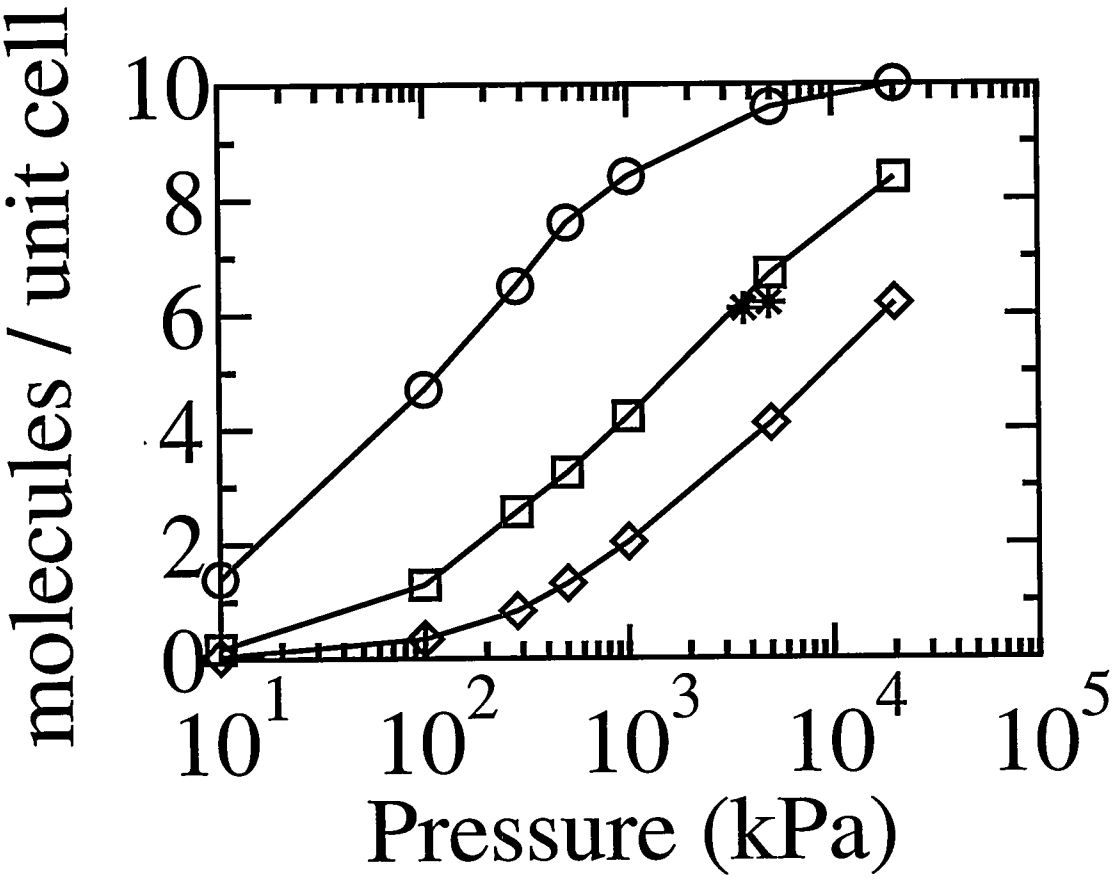

Chandross et al., Fig. 3b

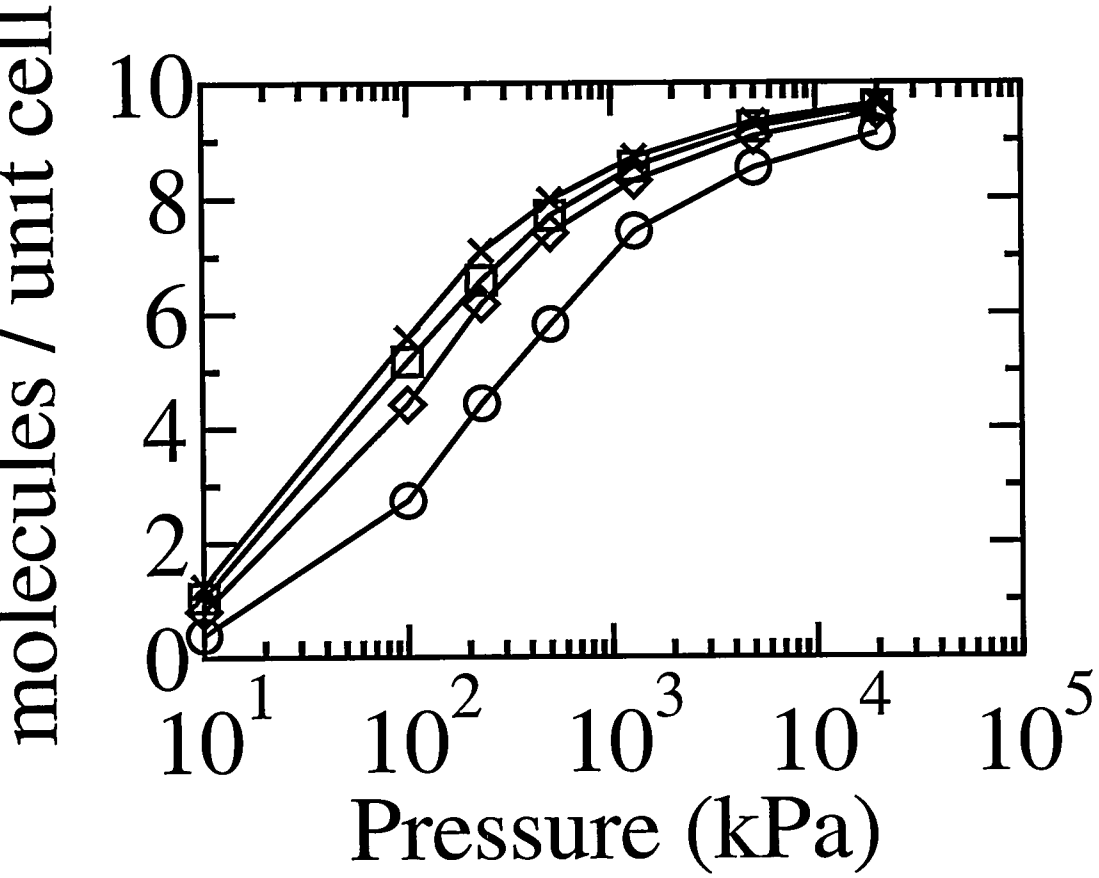

Chandross et al., Fig. 4